No. 32

DESIGN AND RF TUNING OF THE KEK 40 MeV PROTON LINEAR ACCELERATOR

Takao KATO

NATIONAL LABORATORY FOR
HIGH ENERGY PHYSICS

DESIGN AND RF TUNING OF THE KEK 40 MeV PROTON LINEAR ACCELERATOR

Takao KATO

National Laboratory for High Energy Physics

Oho-machi, Tsukuba-gun, Ibaraki-ken, 305, Japan

Abstract

An Alvarez linac was designed and constructed on the basis of a
model linac study to increase the output energy from 20 to 40 MeV. The
linac was tuned by frequency tuners and post couplers. Stabilization
of the field was achieved and a variation within ± 0.7 % of the accel-
erating field was obtained. An equivalent circuit analysis which can
numerically solve loop equations, including stem and post currents in
addition to tank current, can explain the rf characteristics of a post-
coupled structure.

Keywords: proton linear accelerator, rf tuning, post coupler,
              stabilization, equivalent circuit

1. Introduction

A 20-MeV Alvarez linear accelerator was constructed[1] in 1974 and
had delivered a 120-mA stable proton beam for more than eight years.[2,3]
Instead of proton multiturn injection into the Booster synchrotron, H⁻
charge exchange injection was adopted at KEK since June 1985. For the
higher intensity in the Booster, an extension of the linac was planned
so as to increase its output energy from 20 to 40 MeV.[4,5,6] In 1983, a
model linac was built in order to study the rf characteristics of a
post-coupled structure.[7] On the basis of the knowledge of the model
linac, a new linac was designed and constructed. A special feature of
the linac is the utilization of post couplers in order to stabilize and
adjust the field. Stabilization with post couplers was devised by a
Los Alamos group[8] and a lot of studies have been carried out.[9-13] We
utilized an equivalent-circuit analysis in order to explain the rf
characteristics of a post-coupled structure. In this paper, we
describe the results of the model linac study, the design of a new
linac, the tuning of the new linac by both post couplers and frequency
tuners and an analysis with an equivalent circuit.

2. The 20 MeV old linac

2.1 Field distribution of the old linac

The 20-MeV old linac has an inclined field distribution given by

$$E = 1.5 + 0.04 z \ (MV/m) \quad ,$$

where z is the distance along the tank.[14] The inclined field distribu-

tion was achieved by using fourteen frequency tuners. However, there were some deviations from the design field as shown in Fig. 1[14] and Fig. 2.[15] From the view point of field tuning, to flatten the field distribution is as difficult as to incline it. This is one of the reasons for adopting post couplers for flattening the field distribution in the new linac.

2.2 Resonant frequency of the old linac

A resonant frequency of 201.07 MHz during normal operation is different from the design value by 180 kHz; this does not seem small in comparison with the variable-frequency range of the fourteen frequency tuners. This suggests a required frequency range for the frequency tuner of the new linac. A frequency perturbation caused by stems and post couplers (see sections 5.7 and 5.8) also suggests a desirable frequency tuning range.

2.3 Output energy of the old linac

It is an important problem to determine the output energy which equals the injection energy of the new linac. The calibration of the momentum analyzer for proton beams was performed more than a several years ago and has become inadequate. The magnetic field of the Booster Synchrotron during the injection of the beam is related to the linac beam energy and shows rather low values of 20.4 - 20.7 MeV (Fig. 3) compared with the design value of 20.8 MeV for a synchronous particle.[16] A magnetic field of 2000 gauss corresponds to an injection energy of 20.7 MeV. Some confusion regarding the design output energy

was found among refs. (1), (2) and (16). Therefore, various beam dynamics calculations were performed to estimate the output energy of the 20 MeV linac. The results are shown in Fig. 4. The solid curve was calculated from the design field distribution, while the dashed curve from the measured distribution in ref. (15). The latter has some ambiguities in the abscissa arising from an uncertainty in the normalization of the field strength. The computer calculation was performed with 5000 particles that were uniformly distributed in a longitudinal phase space and the average output energy was calculated. The output energy varies with the field strength because of longitudinal oscillation. It is clear that the rather low output energy is due to the perturbed field distribution. An injection energy of 20.6 MeV was chosen.

2.4 Required rf exciting power of the old linac

According to field measurements, the required rf power for the excitation of the design field level was estimated to be 0.968 MW.[14] The above-mentioned estimation was performed with the measured shunt impedance and the design field distribution instead of the measured one. It was shown that the normal operation of the old linac was performed with an exciting rf power of more than 1.2 MW. Therefore, the operation took place with a rather high field level of 1.11, assuming a design field level of 1.0. The reason was an increase in the capture efficiency in order to achieve the calculated capture efficiency at the design field level. The experience of the old linac resulted in an overestimation of the required rf power of the new linac.

3. Design tools

Two computer codes were utilized for calculating the geometry of the linear accelerator.

3.1 SUPERFISH*

SUPERFISH[17] calculates the resonant frequencies, distribution of electromagnetic fields, power dissipation, shunt impedance, Q value and transit time factor of a given geometry of a cylindrical symmetric cavity. Therefore, a set of transit time factors, ratios of gap-to-cell length and shunt impedance as a function of the relevant energy at a given rf frequency can be prepared for the generation of a linac by PARMILA (see section 3.2).

Figure 5 shows the geometry of a drift-tube linac (DTL) where D is the tank diameter, R the corner radius, r the nose radius and 'a' the radius of the beam hole. A unit-cell length is defined in which a particle travels with a period of an rf frequency:

$$L = \beta\lambda \quad .$$

Here, $\beta = v/c$, v = average velocity of a particle in a cell, c = the velocity of light, $\lambda = c/f$ and f = the rf frequency.

Two modifications were made to the original code (version of real*4). The first was an extension of the dimension of the mesh (as large as 20000). The second was to run in double precision in order to decrease any calculation errors (version of real*8).

* SUPERFISH (version of real*4) was brought by Dr. D.A. Swenson in May 1981 and modified to run on the HITAC computer at KEK by him.

- 5 -

A comparison of the results with other computer codes[18] is shown in Table 1 and the corresponding geometries are given in Table 2. Our calculation was performed with a mesh size of 0.5 cm in the axial direction, while it was doubled beyond a distance of 10 cm in the radial direction. Figure 6 shows the mesh-size dependence of the resonant frequency.

3.2 PARMILA**

PARMILA calculates the dimensions of a drift-tube linac on the basis of the results of SUPERFISH. It also calculates the longitudinal and transverse beam dynamics. Four modifications were given to the original code. The first was to run in double precision in order to increase the accuracy. The second was to renew the values of a few natural constants such as the unit charge, the velocity of light, and the proton mass according to the latest authorized values. The third was to compensate for the discrepancy between the resonant frequency of SUPERFISH and the running frequency in PARMILA, which arose from the effect of stems, post couplers and frequency tuners. PARMILA determines a unit-cell length as follows (in principle). A cell length is given by $\beta\lambda$ and the gap length by $\beta\lambda\alpha$, where α is the ratio of the gap to cell length and is a function of beta. Since the frequency of

** PARMILA was brought by Dr. D.A. Swenson in May 1981. Program modules were added together as necessary and modified to run on the HITAC computer by the author. Since there was no reference manual or explanation regarding the code, it was examined and assured to be consistent with the formula in the ref. (19).

- 6 -

SUPERFISH was different from that of PARMILA by 440 kHz in our case; some corrections were needed to relate the resonant frequency in PARMILA with that of SUPERFISH. We defined the virtual β_v as

$$\beta_v = \beta \lambda_p / \lambda_s \quad ,$$

where λ_p and λ_s are wavelength in PARMILA and SUPERFISH, respectively. β_v was utilized only for determining the gap length. A linac designed by PARMILA with the above correction has a resonant frequency equal to that of SUPERFISH. The last modification was to add sub-programs which representated the geometry of a linac, in which the position of the center of each drift tube from the entrance and the length of each drift tube were prepared for the ease during design of construction.

4. Determination of fundamental parameters of a linear accelerator

The purpose is to find the optimum geometry which has a high effective shunt impedance, a high Q value and a low surface electric field. However, there are, in general, some boundary conditions such as the given resonant frequency, a limited rf power, a limited length of the linac, a limited focusing strength of quadrupole magnets installed in drift tubes and some limitations of implement sizes during construction. Therefore, a determination of the unit-cell geometry and the dimensions of a tank needs some compromise between the demand for better rf properties and the restriction given by the boundary conditions mentioned above.

The given limitations are:

1. a resonant frequency of 201.07 MHz,

2. an injection energy of 20.6 MeV,

3. an output energy of more than 40 MeV,

4. an available rf power of less than 1.5 MW,

5. a linac length of less than 15 m,

6. a transverse focusing by permanent quadrupole magnets, which have the maximum field gradient of 25 T/m with a bore radius of 17 mm[20],

7. a distance of 2.5 m between the old linac and the new one, and

8. a utilization of many of the implements for the old linac.

One of the important factors regarding stable operation of a linear accelerator is to prevent the linac from a voltage breakdown. Kilpatrick's criterion[21] is useful for discussing the maximum surface electric field in a linac. Figure 7 shows the frequency dependence of Kilpatrick field limit. It is 14.7 MV/m at a frequency of 200 MHz.

4.1 Tank diameter

Figures 8-12 show the rf properties as a function of the proton energy in terms of $\beta(v/c)$ for tank diameters of 90 and 88 cm. The calculation was performed with a drift tube dimension of d = 16, R = 4, r = 1 and a = 1.5 cm. The resonant frequency was normalized to 201.07 MHz. The important factors are the effective shunt impedance and the maximum surface electric field. In SUPERFISH the maximum surface electric field is given under the condition that the average axial electric field in a cell is assumed to be 1 MV/m. A diameter of 90 cm was chosen because of a lower maximum surface electric field and an easier utilization of the old implements utilized for the old linac which was 94 cm in diameter.

4.2 Drift tube diameter

The diameter of a drift tube has a large influence on the effective shunt impedance (Fig. 13) and the maximum surface electric field (Fig. 14). A small diameter is desirable for a high effective shunt impedance, while a large diameter is desirable for a lower surface electric field. Therefore, a diameter of 16 cm was chosen.

4.3 Corner radius

Figures 15 and 16 show the effects of a corner radius. The smallest length of the drift tubes in the new linac is 23.3 cm and a straight part of more than 16 cm is necessary to install a permanent quadrupole magnet. A corner radius of 4 cm was chosen.

4.4 Nose radius

The effective shunt impedance and the maximum surface electric field as a function of the nose radius are given in Figs. 17-18. A nose radius of 0.5 cm was chosen.

4.5 Bore radius

The trasit-time factor is given by

$$T(r) = \frac{I_0(kr)\sin(\pi g/L)}{I_0(ka)\pi g/L}$$

$$k = (2\pi/\lambda)^2(1/\beta_s^2 - 1)$$

where I_0 is a modified Bessel function, r the radial coordinate, g the gap length and L the cell length. The requirement that the acceleration on the off-axis should be nearly equal to that on the axis limits bore radius:

$$a \ll \beta\lambda/\pi \ .$$

A bore radius of 1.5 cm was chosen with an assurance that the permanent quadrupole magnets of this size are strong enough to keep the beam stable.

4.6 Strength of the accelerating field and the synchronous phase

The strength of the accelerating field determines the longitudinal beam dynamics and the longitudinal acceptance. It also determines the length of the linac and required rf power. In our case, the limited rf available power for stable operation gives the upper limit of the field strength. Figure 19 shows the required rf power as a function of the field strength when the output beam energy is 40 MeV. Figure 20 shows the required linac length as a function of the accelerating field.

A long distance of 2.5 m between the old linac and the new one caused anxiety about longitudinal matching between the two linacs. Therefore, a bunch monitor was developed[22] and a lot of measurements of the 20-MeV beam were performed during 1982 and 1983. Figure 21 shows the bunch length measured at a distance of 4.75 m from the old linac. A calculated bunch length is given in Fig. 22. The longitudinal acceptances of the 20 and 40-MeV linacs on the basis of a design field distribution are given in Fig. 23. Roughly speaking, the phase acceptance is $3|\psi_s|$, where ψ_s is the synchronous phase. Therefore, as the synchronous phase increases the acceptance also increases; at the same

time, the efficiency of the acceleration decreases. An accelerating field of 2.12 MV/m and a synchronous phase of - 30° were chosen. The maximum surface electric field during normal operation becomes 11.1 MV/m; this is much smaller than the Kilpatrick field limit.

5. The model linac

5.1 Design of the model linac

An Aℓ model linac was designed and built for studying the rf characteristics of a post-coupled structure and for finding the frequency deviation from SUPERFISH calculations. A frequency of 400 MHz was chosen because of ease of construction. Table 3 shows the result of PARMILA. Table 4 shows the rearranged result of the calculation and the corresponding cell geometry is given in Fig. 5. In order to make a scale model, the energy gain in a unit cell of the scale model should be equal to that of the master linac. Therefore, a field of 4.4 MV/m was chosen. Figure 24 shows a drawing of the model linac.

5.2 Cylindrical tank without drift tubes

Since one of the purposes of the model linac was to find the frequency deviation from the calculated value, the model was constructed as accurately as possible. Measured TM and TE modes are shown in Fig. 25. The effect of air on the resonant frequency is given by

$$\omega'/\omega = \sqrt{\epsilon/\epsilon'} \quad ,$$

where ϵ' is the relative dielectric constant of air, ϵ that in a vacuum, and ω' the angular frequency in air and ω that in a vacuum. As $\epsilon' = 1.0005$ in air, the decrease of the resonant frequency from that in a vacuum is 100 kHz at a frequency of 400 MHz. Measured resonant frequencies of the TE111 and TM010 modes were 394.78 and 509.9 MHz, smaller than the calculated values based on the measured diameter and length by 0.029 and 0.09 %, respectively.

5.3 Resonant modes with drift tubes

When the drift tubes were installed on the central axis of the tank, the modes of the cylindrical tank became strongly perturbed and their frequencies decreased. The measured dispersion relation is shown in Fig. 26. There are three kinds of modes (TM01, TE11, and stem) modes in the relevent frequency region. Calculated TM01n modes by SUPERFISH are shown in Fig. 27 and Table 5.

5.4 Tuning with post couplers

At first, some frequency perturbations were given to both end cells by adjusting the end plates in order to tilt the field distribution without changing the resonant frequency. Then, post couplers of 15 mm in diameter were uniformly inserted into the tank. The TE11 modes were strongly perturbed and, finally, a number of post modes appeared. As the post length, the distance between a post coupler and a drift tube, decreased, the frequencies of the post modes decreased and when the post band edge crossed the TM010 mode, the field was strongly perturbed. Stabilization was achieved at a post length of

37.6 mm and the field distribution became flat (Fig. 28).

Since the design of the field distribution is uniform, the field stabilization means that the distortion parameter D_x takes a minimum value,

$$D_x = \sum_{i=1,N} |E_i - E_{ave}|$$

and

$$E_{ave} = \frac{1}{N} \sum_{i=1,N} E_i \quad ,$$

where E_i represents the field of the i-th cell and N is the total number of cells.

The measured dispersion relation during stabilization is shown in Fig. 29.

5.5 Tuning with tabs

Elliptical tabs were attached to the inner end of the post couplers. They were turned 360 degrees and moved in and out freely. Three kinds of tabs of different surface areas (Table 6) were prepared for studying the properties of the tabs. Rotation of tab seems to break the symmetry of the configuration of post couplers and drift tubes. This had a large influence on the field distribution (Fig. 30). The post length at the stabilization varied with tab size as if a tab and a drift tube made a capacitor between them as shown in Fig. 31. The post resonant frequency is defined by

$$\omega_2 = 1/\sqrt{L_2 C_2} \quad ,$$

where L_2 is the inductance of a post coupler and C_2 is the capacitance between a post coupler and a drift tube (Fig. 35). The measurements

mentioned above support the validity of the post resonant frequency given by the above formula. The largest tab is desirable because its post length during atabilization is the longest; this increases the reliability of high-power operation.

5.6 Frequency tuner

Four frequency tuners of 62.5 mm in diameter were inserted from the outer wall and aimed at the center of a gap between the drift tubes. They have a stroke of 180 mm and change the TM010 resonant frequency as shown in Fig. 32. The linear region of the left side of the curve in the Fig. 32 is suitable for normal operation. Therefore, the normal position of the 45-mm insertion was selected and the tunable frequency range became ± 305 kHz. In the case that a decrease in the resonant frequency is desirable, a tuning ball that is 30 mm in diameter can be attached to the end of a rod of 12 mm in diameter and is pushed into the gap where the electric field is superior to the magnetic field. A shift of the resonant frequency by the tuning ball is shown in Fig. 33.

5.7 Effect of stems on the resonant frequency

Stems have a large effect on the resonant frequency. Three kinds of stems were prepared in order to determine the frequency shift due to stems. The results are shown in Fig. 34. An average frequency shift of 2.59 kHz per unit cross-sectional area (mm^2) of a stem was obtained. The effect of a stem on the resonant frequency was estimated by G. Parzen.[23] By applying his calculation to a model tank, a shift in the

resonant frequency of 2.96 kHz/mm^2 was obtained; this agreed approxi-
mately with the measurement.

5.8 Summary of the resonant frequency

The measured resonant frequency of the TM010 mode was 401.673 MHz,
while the calculated one was 400.988 MHz. The discrepancy between them
was analyzed as follows:

increase by stems	659 kHz,
increase by post couplers	228 kHz,
increase by tuners	305 kHz, and
decrease by errors	- 507 kHz.

The above figures include a correction factor for air of 100 kHz. In
the above analysis, the decrease by errors is mainly due to the effect
of the mesh size used in a SUPERFISH calculation.

5.9 Effects of stems and post couplers on the field distribution

A stem and a post coupler are inserted from the outer wall for
each cell. The length of a unit cell increases as the velocity of the
beam increases. Therefore, the frequency perturbation caused by a stem
and a post coupler varies with the cells, producing a variation in the
field distribution. There are three possible solutions to the problem.
The first is to calculate a unit cell which includes the effect of fre-
quency perturbation by both a stem and a post coupler. Then, the reso-
nant frequencies of a SUPERFISH calculation differ from cell to cell.
The second is to make stems and post couplers so that their perturba-
tions are kept constant along the tank. Therefore, their diameters

vary along the tank. The third is to correct the inclined field dis-
tribution by some other method (for example, by uitlizing the frequency
tuners or stabilization of the field). The last method was adopted
since the linac length was not so long and their perturbations were not
so large and could be corrected by frequency tuners. Furthermore,
according to the results of a model linac study, stabilization by post
couplers can adjust the perturbed field easily (Figs. 28 and 30).

5.10 Summary for the design of the 40-MeV linac

The results of the 400-MHz model linac study were applied to the
design of a 200-MHz linac. The resonant frequency of the calculation
was determined as:

increase by stems	330 kHz,
increase by post couplers	114 kHz,
increase by tuners	179 kHz,
decrease by errors	- 253.5 kHz, and
safety factor	- 70 kHz.

Then, the calculated frequency was assumed to be 200.63 ± 0.001 MHz,
while the goal of the frequency was 201.07 MHz. A safety factor of -
70 kHz arose from the fact that an increase in the resonant frequency
was easier than a decrease.

6. Structure of the 40 MeV linac

PARMILA calculated the dimensions of the new linac according to
the table of parameters given by SUPERFISH. Tables 7 - 9 show the

results of the calculation.

A new linac of 0.9 m in diameter and 12.844 m in length consists of four sub-tanks and contains thirtyfour-full drift tubes and two half drift tubes at the ends. The geometry of the 40-MeV linac is given in Table 10. The ratio of the gap-to-cell length changes from 0.2456 to 0.3187. Twelve frequency tuners were prepared in order to shift the resonant frequency and to locally change the field. Furthermore, two frequency tuners were prepared to automatically tune the resonant frequency to the old linac with a feedback circuit. Thirty four post couplers were alternately installed from both sides of the tank toward the center of the drift tube. Elliptical tabs were attached to the inner ends of post couplers. They can turn 180 degrees and move in and out by about 160 mm. Two rf loop couplers (located at 1/4 and 3/4 of the linac) were utilized to deliver rf power.

7. Equivalent circuit analysis

The equivalent circuit used[9] is shown in Fig. 35. Notations in Fig. 35 follow ref. (11). There are six unknowns: the tank current of the TM-like mode $I(n,1)$, three stem currents $I(n,2)$, $I(n,3)$ and $I(n,4)$ and two post currents $I(n,5)$ and $I(n,6)$ for the n-th circuit. The total number of unknowns for an N-coupled chain is $6(N-1) + 1$. Then, $(6N-5)$ equations can be numerically solved to obtain three kinds of currents: $I_{tank}(n) = I(n,1)$, $I_{stem}(n) = I(n,2) + I(n,3) + I(n,4)$ and $I_{post}(n) = I(n,5) + I(n,6)$. Using Kirchhoff's law, the loop equations for the n-th circuit can be written as

$$V_{c,n} = I(n,2)/2j\omega C_1 \quad , \tag{1}$$

$$V_{c,n} - V_n = j\omega L_0(1 - \omega_0^2/\omega^2)I(n,1) + J\omega M_0 I(n+1,1) \quad , \tag{2}$$

$$V_{n+1} - V_{c,n} = j\omega L_0(1 - \omega_0^2/\omega^2)I(n+1,1) + J\omega M_0 I(n,1) \quad , \tag{3}$$

$$V_{c,n} = j\omega L_1 I(n,3) + j\omega M_1 I(n-1,4) \quad , \tag{4}$$

$$V_{c,n} = j\omega L_1 I(n,4) + j\omega M_1 I(n+1,3) \quad , \tag{5}$$

$$V_{c,n} = j\omega L_2 I(n,5) + I(n,5)/j\omega C_2 + j\omega M_2 I(n-1,6) \quad , \tag{6}$$

$$V_{c,n} = j\omega L_2 I(n,6) + I(n,6)/j\omega C_2 + j\omega M_2 I(n+1,5) \quad , \tag{7}$$

and

$$I(n+1,1) = \sum_{m=1,6} I(n,m) \quad . \tag{8}$$

In the above, $\omega_0^2 = 1/L_0 C_0$ and ω is the driving frequency. If equations from (2) to (7) are rearranged using equation (1), and if equation (3) for the (n-1)-th circuit and equation (2) for the n-th circuit are added together, the following equations are obtained for the n-th circuit:

$$2(1 - \omega_0^2/\omega^2)I(n,1) + (\omega_1^2/2\omega^2)I(n,2)$$
$$- (\omega_1^2/2\omega^2)I(n-1,2) + k_0 I(n-1,1) + k_0 I(n+1,1) = 0 \quad , \tag{9}$$

$$(\omega_3^2/2\omega^2)I(n,2) + I(n,3) + k_1 I(n-1,4) = 0 \quad , \tag{10}$$

$$(\omega_3^2/2\omega^2)I(n,2) + I(n,4) + k_1 I(n+1,3) = 0 \quad , \tag{11}$$

$$I(n,3) - k_4(1 - \omega_2^2/\omega^2)I(n,5) + k_1 I(n-1,4) - k_2 I(n-1,6) = 0 \quad , \tag{12}$$

$$I(n,4) - k_4(1 - \omega_2^2/\omega^2)I(n,6) + k_1 I(n+1,3) - k_2 I(n+1,5) = 0 \quad , \tag{13}$$

and

$$I(n+1,1) = \sum_{m=1,6} I(n,m) \quad . \tag{14}$$

Here, $k_0 = M_0/L_0$, $k_1 = M_1/L_1$, $k_2 = M_2/L_1$, $k_4 = L_2/L_1$, $\omega_1^2 = 1/L_0 C_1$, $\omega_2^2 =$

$1/L_2C_2$ and $\omega_3^2 = 1/L_1C_1$.

A computer code was written on the basis of equations (9) - (14). Calculated currents were so normalized that the largest one among the three kinds of currents in the circuits was assumed to be 1.

8. Measurement method

8.1 Axial field distribution

The axial field was measured by the bead perturbation method. Figure 36 shows a block diagram of the measurement. Some care was taken to increase the accuracy. A phase-locked loop was utilized for stabilizing the speed of the bead. Its fluctuation could be reduced to less than 0.01 %. The resonant frequency of the self-excited circuit, including the linac, was stabilized with a suitable gain and the phase of the feedback amplifiers. A reference frequency producing a beat frequency of 8 kHz was delivered from a synthesized oscillator. Clock pulses for driving the motor and counting the beat frequency were supplied by stable oscillators. Two photo-sensors were utilized to detect the passing of the bead. They determined the location of the bead in the linac with the aid of 10-MHz clock pulses. The error of the measurement of the field averaged over a unit cell was less than 0.2 %.

We used another method for an axial field measurement; this method is simple and useful when we wanted to identify the mode. If an external driving frequency is fixed on the shoulder of a resonant curve (for example, - 3 dB down from center of a curve) a shift of the reso-

nant frequency by the bead perturbation causes a change in the amplitude of the measured rf signal. A synthesized network analyzer[*] with a fixed driving frequency measures the signal with high accuracy.

8.2 Q value

An unloaded Q value was obtained by measuring - 3dB down frequencies on the resonant curve and using

$$Q_L = f/\Delta f$$

and

$$Q_0 = (1 + \beta_1 + \beta_2)Q_L ,$$

where Q_L is the loaded Q value, Q_0 the unloaded Q value, β_1 the coupling coefficient of the input port, β_2 that of the output port, f the resonant frequency and Δf the separation between - 3 dB down frequencies. Two coupling coefficients were calculated from the power relation:

$$\beta_2 = \frac{P_{tr}}{P_{in} - P_{ref} - P_{tr}} ,$$

if $\beta_1 < 1 + \beta_2$

$$\beta_1 = (1 + \beta_2) \frac{1 - \sqrt{P_{ref}/P_{in}}}{1 + \sqrt{P_{ref}/P_{in}}} ,$$

and if $\beta_1 > 1 + \beta_2$

$$\beta_1 = (1 + \beta_2) \frac{1 + \sqrt{P_{ref}/P_{in}}}{1 - \sqrt{P_{ref}/P_{in}}} .$$

* MS620J, Anritsu corporation.

In these equations, P_{in} is the input rf power, P_{ref} the reflected power and P_{tr} the transmitted power. In order to eliminate the effects of a mismatch of rf components and coupling coefficients we measured the transmitted rf power with low coupling coefficients and a sensitive detector which could detect as low as 0.1 nW. As a matter of course, the measured Q_0 with one rf port and a large coupling coefficient agreed with that with two rf ports and small coupling coefficients whenever careful measurements were performed. However, it seemed easier to measure the Q value with two ports and coupling coefficients that were as small as possible.

9. Measurements on the 40-MeV linac

9.1 Cylindrical sub-tank without drift tubes

The inner surfaces of the tanks were copper-plated to a thickness of 500 μm. The TM010 resonant frequencies and the Q values of the four sub-tanks were measured before installing the drift tubes. Table 11 shows the results. Their measured diameters were the average values of the twenty different places in the tank. A number of large holes on the wall for frequency tuners and rf couplers were compensated with Aℓ blocks during measurements. A decrease in the resonant frequency due to small holes for the installation of stems and post couplers was estimated on the basis of experimental results from the model linac. Since Aℓ end plates were utilized for all the tanks, it is not so important to compare the measured Q and calculated values.

9.2 Cylindrical sub-tank with drift tubes

The TM010 resonant frequencies and the Q values of the sub-tanks were measured after installing the drift tubes and post couplers. The post length was 160 mm, which meant they were pulled out exceedingly. The results are given in Table 12. Except for the copper-plated end plate utilized for the No.7 and No.10 tanks, Aℓ end plates were utilized during the measurements.

9.3 Tuning procedures

There are two important problems regarding the tuning of the tank: one is the stabilization of the field with post couplers, and the other is the method for tuning the resonant frequency to 201.07 MHz (the value for the old linac). The latter is important since the initial field distribution adjusted by frequency tuners affects the amount of excitation of the post modes when stabilization is achieved (as shown in section 10.2). Therefore, care was taken to obtain a field distribution that was as flat as possible while keeping a resonant frequency of 201.07 MHz of the evacuated tank and avoiding any excitation of stem and post modes (as small as possible) during stabilization.

9.3.1 Accelerating field without post couplers

Figure 37 shows the measured field distribution of the TM010 mode when post couplers were pulled out excessively (155 mm away from the drift tubes). The field distribution became inclined due to the effect of the stems and post couplers and $D_x = 0.14$. In the design of the

linac, the average effects of stems and post couplers on the resonant frequency were taken into account; thus, all cells were calculated with the same frequency. The result of a calculation using an equivalent circuit is also shown. The frequency perturbations due to stems and post couplers were given in such a way that the frequency deviation from the resonant frequency of a unit cell varied at a uniform rate (from 110 to -110 kHz) in the circuit.

Secondly, fourteen frequency tuners were carefully inserted in order to obtain a nearly uniform field distribution (Fig. 38); D_x became 0.0114. Table 13 shows the insertion length of the tuners. Then, a 10 % tilt (Fig. 39) was given to the field distribution by the No.1 and No.12 frequency tuners while keeping the resonant frequency constant; D_x was 0.0306. The above procedure was useful for clearly determining the stabilizing point. A dispersion relation for the post-less linac is shown in Fig. 40. The measured resonant modes are shown in Fig. 41.

9.3.2 Tuning with post couplers

As the post couplers were uniformly inserted into the tank, TE11 modes were strongly perturbed and, finally, a number of post modes appeared as shown in Fig. 42. As the post length decreased, the frequencies of the post modes decreased; and when the post band edge crossed the TM010 mode, the field became strongly perturbed (Fig. 43). Stabilization was achieved at a post length of 74 mm and the field distribution became flat as shown in Figs. 44 and 45. D_x was 0.00886.

9.3.3 Tuning with tab rotation

With the aid of the small tab rotation of five post couplers given in Table 14, a distortion parameter of 0.0029 was achieved and a field variation within ± 0.7 % was obtained (Figs. 46, 47 and Table 15). The field distribution was sensitive to tab rotation and was reproducible with tab rotation, which was useful for determining the accuracy of the field measurement. The dispersion relation during the stabilization is shown in Fig. 48. The observed resonant modes are shown in Fig. 49. Some of them are listed in Table 16. The mode separation between TM010 and TM011 increased from 0.3 to 1.57 MHz after stabilization. Figure 50 shows the variation in the distortion parameter while tuning post couplers. The variation of R/Q and the resonant frequency of the TM010 mode are shown in Figs. 51 and 52.

9.3.4 Post modes

In addition to the stem modes ranging from 73 to 81 MHz, thirty four resonant modes, corresponding to the post modes (Fig. 53), were observed below the TM010 mode. Figure 54 shows the measured rf amplitude of the TM013, TM011, TM010, post-1 and post-2 modes with a bead perturbation on the axis during stabilization. Since the lower side of the shoulder of resonant curve was utilized in the measurement, the upward signal from the base line meant that an electric field was dominant in the gap. In the measurement of TE modes, both upward and downward signals appeared alternately. This feature makes it easy to identify the mode.

9.3.5 Effect of frequency tuners

The frequency tuners vary not only the resonant frequency but also the field distribution due to the local frequency perturbation. Although the field was stabilized by the post couplers, a slight change of the field distribution was observed (Fig. 55 and Fig. 56). Shift of the resonant frequency by twelve tuners and auto-tuners are shown in Figs. 57 and 58, respectively. An insertion length of 47 mm is regarded as a tuner length of zero for auto-tuners.

9.3.6 Tuning of the two rf input couplers

The new linac, as well as the old one, utilizes two rf input couplers (located at 1/4 and 3/4 of the tank). Each rf coupler is coupled to the linac with a coupling coefficient of 1.0. This can be achieved by attaching the two rf couplers so that the transmitted and reflected fields at the port add 180° out of phase and are equal in amplitude. Figure 59 shows a polar view of the rf ports at the matched position of the rf couplers. In the above measurements, the other port was terminated in a matched load impedance or a open-circuit termination. Thus, the coupling coefficient of the driving port seemed to be less than 1. Figure 60 shows the relative field level of the linac and the voltage-reflection coefficients of the two ports as a function of the phase errors of one port (in the case of a two-feed operation). Some discrepancies between the reflection coefficients were due to tuning errors of the rf couplers.

9.3.7 Calibration of rf monitor couplers

Calibration of seventeen rf monitor couplers was performed using a two-feed operation with matched rf input couplers and a high sensitivity rf power meter. Figure 61 shows the measured attenuation of the transmitted rf power as a function of the extraction length of the monitor coupler. They were adjusted to have an attenuation of - 66 dB.

9.4 Resonant frequency of the TM010 mode

The model linac study predicted a deviation of the resonant frequency from the SUPERFISH calculation (see section 5.10). The deviation of the resonant frequencies from the estimated value was -2 kHz for the post-less linac and -10 kHz for the stabilized linac (provided that any changes in the resonant frequency due to temperature or atmosphere were -2.9 kHz/degree and 62 kHz, respectively). Since the contribution of the dielectric constant of air was estimated to be 50 kHz, an extra increase of the frequency (12 kHz) might have been due to air moisture (34 %).

9.5 Q values of the 40-MeV linac

The Q value varied during post tuning as:

post-less tank	64900,
decrease by 12 tuners	- 2500,
decrease by auto-tuners	- 1400,
decrease by post couplers	- 3900,
stabilized tank	57100, and
calculation without stems	79100.

9.6 Shunt impedance of the 40 MeV linac

The quantity of R/Q can be calculated using

$$\frac{R}{Q_0} = \frac{2}{3\pi\epsilon_0 f V} \sum_n \frac{1}{L_n} \left(\sum_i (-\frac{\Delta f_i}{f})^{1/2} \Delta Z_i \right)^2 \quad ,$$

where ϵ_0 is the free-space dielectric constant, f the resonant frequency, V the volume of the bead, n the cell number, L_n the n-th cell length, Δf_i the shift in the resonant frequency by the bead perturbation of the i-th measurement and ΔZ_i the length through which the bead travels between successive measurements. The summation over i is taken during measurements of the n-th cell. The average shunt impedance R is defined as follows:[14]

$$R = \frac{1}{P_c} \sum_n \frac{1}{L_n} (E_{0n} L_n)^2 \quad ,$$

where P_c is the dissipation power in the linac and E_{0n} the average accelerating field of the n-th cell.

The shunt impedance of the stabilized tank is 46 MΩ/m. Therefore, the required rf power for the operation of a 1.0 field level was estimated to be 1.25 MW, while the calculated rf power by PARMILA is 1.078 MW (including a multiplying factor of 1.3 compared with an ideal linac made of pure copper).

9.7 Transit-time factor of the 40-MeV linac

Transit-time factors were calculated on the basis of field measurements and are given in Table 15 and Fig. 62. They are larger than the calculated values given in Table 15 by 0.69 % (on the average).

10. Simulation using equivalent circuit

10.1 Equivalent circuit for the 40 MeV post-less linac

Parameters of an equivalent circuit for a 35-cell post-less linac were determined so that several resonant frequencies of TM-like modes near the TM010-like mode, both resonant frequencies and the band width of the stem modes were adjusted to those of the new linac. Figure 63 shows the calculated sums of $I_{tank}(n)$ and $I_{stem}(n)$ as a function of a drive frequency with the parameters of $\omega_0 = 210.8$, $\omega_1 = 215.8$, $\omega_3 = 93$, $k_0 = 0.1$, $k_1 = 0.095$ and $k_4 = 0.71$. Figure 64 shows examples of a field distribution. Table 17 shows a comparison of the calculated and measured TM01-like resonant frequencies.

10.2 Equivalent circuit for the 40 MeV post-stabilized linac

Parameters related to post couplers were introduced so that the stabilization might be achieved and the band width of the post mode might be adjusted to the measured value. Figure 65 shows calculated sums of $I_{tank}(n)$, $I_{stem}(n)$ and $I_{post}(n)$ at the stabilization with parameters of $\omega_2 = 142.4$, $k_2 = -0.09$ and $\omega = 201.00$. The other parameters are the same as those in section 10.1.

The equivalent circuit well explains the behavior of the distortion parameter during post tuning (Fig. 66). Figure 67 shows the calculated sums of the squares of $I_{tank}(n)$ and $I_{post}(n)$ as a function of post drive frequency, which corresponds to the measured R/Q shown in Fig. 51.

The excitation of the post modes during stabilization depends on

the field distribution before post tuning (Fig. 68). In the calculation, the post currents are summed when the initially tilted field distribution due to perturbations given to both end circuits becomes stabilized.

Acknowledgement

The author wishes to express his gratitude to Prof. S. Fukumoto for his valuable discussions and encouragement. He thanks Dr. D.A. Swenson for introducing the valuable computer codes. He also thanks Mr. S. Machida for many discussions and help during measurements and assistance during computer work. He thanks Dr. E. Takasaki, members of the injector group and Mr. Y. Iino and his group of the Mitsubishi Heavy Industry for their help during measurements. He thanks Dr. K. Oide for his assistance in the development of the computer calculation.

References

1. J. Tanaka, "The status of accelerator developments in Japan", Proc. 1976 proton linear accelerator conf., 27 (1976).

2. J. Tanaka et al., "Operation of the KEK 20 MeV injector linac", Proc. 1976 proton linear accelerator conf., 333 (1976).

3. S. Anami et al., "Status of the KEK injector linac", Proc. 1979 linear accelerator conf., 94 (1979).

4. S. Fukumoto et al., "Linac upgrading and P to H⁻ conversion", Proc. 1984 linear accelerator conf., 135 (1984).

5. S. Fukumoto et al., "Design of 40 MeV Alvarez linac", Proc. 5-th symposium on accelerator science and technology", 53 (1984).

6. S. Fukumoto et al., "KEK PS injector linac upgrading", IEEE Trans. Nucl. Sci., NS-32, 3181 (1985).

7. S. Machida, T. Kato and S. Fukumoto, "Measurements on the post stabilized linac", Proc. 5-th Symposium on accelerator science and technology, 83 (1984).

8. D.A. Swenson et al., "Stabilization of the drift tube linac by operation in the $\pi/2$ cavity mode", Proc. 6-th International Conf. on high energy accelerators, CEAL-2000, 167 (1967).

9. T. Nishikawa, "A note on the dispersion relation of the Los Alamos structure for the drift tube linac", 1967, unpublished.

10. C.W. Owen and J.D. Wildenradt, "Experiences with post coupler stabilized structures in the NAL linac", Proc. 1970 proton linear accelerator conf., 315 (1970).

11. G. Dome. "Review and survey of accelerating structures", Linear accelerators edted by P.M. Lapostolle and A.L. Septier, C.1.1e, 706 (1970).

12. J. Ungrin, S.O. Schriber and R.A. Vokes, "Post coupler studies for Alvarez tanks to be used for high power or variable energy", Proc. 1981 linear accelerator conf., 183 (1981).

13. J. Ungrin, S.O. Schriber and R.A. Vokes, "Post-coupler and stem current measurements for high current cw drift-tube linacs", IEEE Trans. Nucl. Sci. NS-30, 3013 (1983).

14. S. Okumura and D.A. Swenson, "Bead perturbation measurement for the KEK linac cavity", KEK-74-15 (1974).

15. S. Inagaki et al., "Field measurement of the KEK linac-cavity by bead perturbation method", KEK-79-7 (1979).

16. J. Tanaka et al., "Synchronous phase law experiment in the KEK linac", KEK-77-3 (1977).

17. H.C. Hoyt, D.D. Simmonds and W.R. Rich, "Computer designed 805 MHz proton linac cavities", Rev. Sci. Instr. $\underline{37}$, 755 (1966).

18. K. Halbach, R.F. Holsinger, W.E. Jule and D.A. Swenson, "Properties of the cylindrical rf cavity evaluation code SUPERFISH", Proc. 1976 proton linear accelerator conf., 122 (1976).

19. A. Carne et al., "Numerical methods, Accelerating gap", Linear accelerators edited by P.M. Lapostolle and A.L. Septier, C.1.2b (1970).

20. E. Takasaki et al., "Permanent quadrupole magnets for drift tubes of 20 - 40 MeV linac", Proc. 5-th Symposium on accelerator science and technology, 206 (1984).

21. W.D. Kilparick, "Criterion for vacuum sparking designed to include both rf and dc", Rev. Sci. Instrum. $\underline{28}$, 824 (1957),
    S.W. Williams et al., "Voltage breakdown in a 420 MHz RFQ structure", IEEE Trans. Nucl. Sci. $\underline{NS-28}$, 2976 (1981).

22. Z. Igarashi et al., "Observation of the beam structure in 20 MeV linac", Proc. 7th meeting on linear accelerator (KEK 82-14), 89 (1983).

23. G. Parzen, "Perturbations and tolerances in a 200-MeV proton linac", Proc. 6-th Int. Conf. on High Energy Accelerators, CEAL 2000, A-34 (1967).

Table 1   Comparison of the calculated results

DTL 20 MeV

	MMESH	SFISH	REAL*4	REAL*8
f_0	200.781	200.839	198.965	200.882
Q_0	85552	86073	85631	86097
Z	70.89	71.22	72.17	70.52
T	0.854	0.864	0.864	0.864
T'	0.044	0.041	0.041	0.041
S	0.427	0.414	0.413	0.413
S'	0.056	0.055	0.055	0.055

DTL 40 MeV

	MMESH	SFISH	REAL*4	REAL*8
f_0	200.806	200.974	198.214	200.912
Q_0	83074	83580	82910	83493
Z	68.18	68.72	70.24	67.99
T	0.800	0.808	0.810	0.810
T'	0.059	0.057	0.057	0.057
S	0.503	0.495	0.494	0.494
S'	0.062	0.062	0.069	0.062

Table 2   Drift tube geometries[18]

Proton energy	20	40	MeV
Cell length	30.708	42.620	cm
Cell diameter	90	90	
Gap length	7.632	13.663	
D.T. diameter	16	16	
Corner radius	4	4	
Nose radius	1	1	
Bore radius	1.5	1.5	

Table 3   Calculated results of the model linac by PARMILA.

TANK NO.   1   TANK LENGTH   251.14433 CENTIMETERS   15 CELLS   POWER= 0.637 MW   COST= 0.0   M¥

CELL NUMBER	KINETIC ENERGY	BETA	LENGTH	T	TP	S	SP	QUAD LENGTH	QUAD GRADIENT	EZERO MV/M	Z	TOTAL LENGTH	RFPOW
NITIAL	20.6000	0.2062						7.0000	6.1195			0.0	
1	21.1102	0.2086	15.4809	0.8650	0.0410	0.4120	0.0550	7.0000	-6.1228	4.4000	99.1914	15.481	0.030
2	21.6250	0.2111	15.6637	0.8625	0.0420	0.4160	0.0555	7.0000	6.1261	4.4000	100.1355	31.145	0.060
3	22.1443	0.2135	15.8456	0.8600	0.0430	0.4200	0.0560	7.0000	-6.1294	4.4000	101.0689	46.990	0.091
4	22.6689	0.2159	16.0270	0.8590	0.0430	0.4220	0.0560	7.0000	6.1327	4.4000	100.8855	63.017	0.122
5	23.1988	0.2183	16.2079	0.8580	0.0430	0.4240	0.0560	7.0000	-6.1361	4.4000	100.7025	79.225	0.153
6	23.7343	0.2208	16.3884	0.8575	0.0430	0.4245	0.0560	7.0000	6.1395	4.4000	99.8064	95.614	0.185
7	24.2754	0.2232	16.5684	0.8570	0.0430	0.4250	0.0560	7.0000	-6.1430	4.4000	98.9022	112.182	0.217
8	24.8220	0.2256	16.7480	0.8565	0.0430	0.4265	0.0565	7.0000	6.1465	4.4000	98.3151	128.930	0.250
9	25.3741	0.2280	16.9273	0.8560	0.0430	0.4280	0.0570	7.0000	-6.1500	4.4000	97.7300	145.857	0.284
10	25.9304	0.2304	17.1057	0.8535	0.0440	0.4315	0.0570	7.0000	6.1535	4.4000	98.3126	162.963	0.317
11	26.4909	0.2327	17.2834	0.8510	0.0450	0.4350	0.0570	7.0000	-6.1571	4.4000	98.8926	180.246	0.351
12	27.0564	0.2351	17.4605	0.8500	0.0450	0.4370	0.0575	7.0000	6.1607	4.4000	98.6758	197.707	0.385
13	27.6270	0.2375	17.6371	0.8490	0.0450	0.4390	0.0580	7.0000	-6.1644	4.4000	98.4517	215.344	0.420
14	28.2012	0.2398	17.8128	0.8460	0.0460	0.4430	0.0580	7.0000	6.1680	4.4000	99.0776	233.157	0.455
15	28.7790	0.2421	17.9876	0.8430	0.0470	0.4470	0.0580	7.0000	-6.1717	4.4000	99.7002	251.144	0.490

Table 4   Rearranged results of the model linac calculated by PARMILA.

CELL NUMBER	KINETIC ENERGY	BETA	STEM LENGTH IN CM	TOTAL LENGTH IN CM	TUBE LENGTH IN CM
	20.59999	0.20617			5.79127
1	21.11024	0.20862	15.47598	15.47598	11.69309
2	21.62502	0.21107	15.66363	31.13961	11.79257
3	22.14428	0.21350	15.84617	46.98578	11.89194
4	22.66889	0.21593	16.02693	63.01271	11.99153
5	23.19880	0.21834	16.20856	79.22126	12.09149
6	23.73429	0.22076	16.38829	95.60955	12.19196
7	24.27535	0.22317	16.56711	112.17666	12.28908
8	24.82196	0.22557	16.74797	128.92464	12.38267
9	25.37409	0.22797	16.92832	145.85296	12.47747
10	25.93043	0.23035	17.10567	162.95863	12.57335
11	26.49090	0.23273	17.28237	180.24100	12.66616
12	27.05644	0.23510	17.46043	197.70143	12.75595
13	27.62702	0.23746	17.63726	215.33869	12.84515
14	28.20124	0.23981	17.81274	233.15143	12.93363
15	28.77905	0.24214	17.99290	251.14433	6.51581

Table 5

Comparison of measured and calculated

TM01n modes of the model linac

mode number n	calculation	measurement
0	401.895	401.38
1	406.245	405.74
2	418.929	417.34
3	439.272	436.35
4	466.302	462.08
5	498.779	493.42
6	535.838	529.42
7	576.419	569.18
8	619.863	611.65
9	665.443	655.73
10	712.632	701.35
11	760.797	775.29
12	808.903	815.19
13	853.426	860.35
14	890.638	

Table 6

Three kinds of tabs

	area (mm*2)
tabless	176.7
small tab	311.7
large tab	551.7

Table 7   Calculated results of the 40 MeV linac by PARMILA.

TANK NO.   1   TANK LENGTH   1284.41703 CENTIMETERS   35 CELLS   POWER=   1.078 MW

CELL NUMBER	KINETIC ENERGY	BETA	LENGTH	T	TP	S	SP	QUAD LENGTH	QUAD GRADIENT	EZERO MV/M	Z	TOTAL LENGTH	RFPOW
INITIAL	20.6000	0.2062						16.0000	-2.1739			0.0	
1	21.0936	0.2085	30.9074	0.8699	0.0393	0.4064	0.0547	16.0000	2.1744	2.1200	70.3300	30.907	0.020
2	21.5923	0.2109	31.2610	0.8690	0.0396	0.4080	0.0549	16.0000	-2.1751	2.1200	70.0726	62.168	0.040
3	22.0946	0.2133	31.6130	0.8654	0.0406	0.4135	0.0554	16.0000	2.1758	2.1200	71.4314	93.781	0.060
4	22.6018	0.2156	31.9637	0.8643	0.0410	0.4155	0.0556	16.0000	-2.1766	2.1200	71.3030	125.745	0.080
5	23.1136	0.2180	32.3132	0.8626	0.0414	0.4183	0.0559	16.0000	2.1774	2.1200	71.3949	158.058	0.100
6	23.6309	0.2203	32.6619	0.8627	0.0414	0.4186	0.0559	16.0000	-2.1782	2.1200	70.5829	190.720	0.121
7	24.1532	0.2226	33.0098	0.8618	0.0417	0.4201	0.0561	16.0000	2.1791	2.1200	70.2109	223.730	0.142
8	24.6811	0.2250	33.3572	0.8620	0.0417	0.4203	0.0562	16.0000	-2.1799	2.1200	69.2983	257.087	0.164
9	25.2120	0.2273	33.7029	0.8580	0.0428	0.4260	0.0566	16.0000	2.1807	2.1200	70.6341	290.790	0.185
10	25.7470	0.2296	34.0469	0.8559	0.0434	0.4293	0.0569	16.0000	-2.1816	2.1200	70.9691	324.837	0.207
11	26.2871	0.2319	34.3899	0.8553	0.0436	0.4305	0.0571	16.0000	2.1825	2.1200	70.4259	359.227	0.229
12	26.8318	0.2342	34.7320	0.8543	0.0439	0.4329	0.0573	16.0000	-2.1834	2.1200	70.1139	393.959	0.251
13	27.3811	0.2364	35.0731	0.8530	0.0443	0.4346	0.0575	16.0000	2.1843	2.1200	69.8997	429.032	0.274
14	27.9355	0.2387	35.4133	0.8528	0.0443	0.4350	0.0576	16.0000	-2.1853	2.1200	69.1718	464.445	0.297
15	28.4933	0.2410	35.7521	0.8498	0.0452	0.4392	0.0579	16.0000	2.1862	2.1200	69.8331	500.197	0.320
16	29.0544	0.2432	36.0892	0.8468	0.0461	0.4435	0.0582	16.0000	-2.1871	2.1200	70.5005	536.287	0.343
17	29.6201	0.2455	36.4250	0.8459	0.0463	0.4450	0.0584	16.0000	2.1881	2.1200	70.0492	572.712	0.366
18	30.1904	0.2477	36.7599	0.8450	0.0466	0.4466	0.0585	16.0000	-2.1891	2.1200	69.6493	609.471	0.390
19	30.7649	0.2500	37.0937	0.8436	0.0470	0.4487	0.0587	16.0000	2.1902	2.1200	69.4563	646.565	0.414
20	31.3441	0.2522	37.4265	0.8429	0.0472	0.4499	0.0589	16.0000	-2.1912	2.1200	68.8969	683.992	0.438
21	31.9270	0.2544	37.7581	0.8409	0.0478	0.4527	0.0591	16.0000	2.1922	2.1200	68.9897	721.750	0.463
22	32.5124	0.2566	38.0879	0.8371	0.0489	0.4578	0.0594	16.0000	-2.1932	2.1200	69.9452	759.838	0.487
23	33.1020	0.2588	38.4163	0.8360	0.0492	0.4595	0.0596	16.0000	2.1943	2.1200	69.5859	798.254	0.512
24	33.6961	0.2610	38.7437	0.8351	0.0494	0.4609	0.0597	16.0000	-2.1954	2.1200	69.1047	836.998	0.537
25	34.2940	0.2632	39.0700	0.8336	0.0499	0.4631	0.0599	16.0000	2.1965	2.1200	68.9239	876.068	0.563
26	34.8955	0.2654	39.3951	0.8316	0.0504	0.4658	0.0601	16.0000	-2.1976	2.1200	68.9546	915.463	0.588
27	35.4996	0.2675	39.7184	0.8284	0.0514	0.4700	0.0604	16.0000	2.1987	2.1200	69.5525	955.181	0.614
28	36.1074	0.2697	40.0402	0.8268	0.0518	0.4722	0.0606	16.0000	-2.1998	2.1200	69.3826	995.221	0.640
29	36.7187	0.2718	40.3608	0.8250	0.0523	0.4747	0.0608	16.0000	2.2009	2.1200	69.2922	1035.582	0.666
30	37.3347	0.2740	40.6805	0.8247	0.0524	0.4753	0.0608	16.0000	-2.2021	2.1200	68.5590	1076.263	0.693
31	37.9544	0.2761	40.9992	0.8233	0.0528	0.4773	0.0610	16.0000	2.2033	2.1200	68.3338	1117.262	0.720
32	38.5777	0.2783	41.3167	0.8216	0.0533	0.4795	0.0612	16.0000	-2.2045	2.1200	68.1726	1158.579	0.747
33	39.2029	0.2804	41.6324	0.8180	0.0543	0.4840	0.0614	16.0000	2.2056	2.1200	68.8974	1200.211	0.774
34	39.8317	0.2825	41.9466	0.8165	0.0548	0.4860	0.0616	16.0000	-2.2068	2.1200	68.6880	1242.158	0.802
35	40.4635	0.2846	42.2595	0.8143	0.0554	0.4889	0.0617	16.0000	2.2080	2.1200	68.7139	1284.417	0.829

Table 8   Detailed geometry of the 40 MeV linac calculated by PARMILA.

DTL DETAIL

CELL NUMBER	KINETIC ENERGY	BETA	XL	XR	CELL LENGTH	TOTAL LENGTH	DD1	DD2	GAP LENGTH	DQ1	DQ2	DTL1 LENGTH	DTL2 LENGTH	G/L
INPUT	20.600	0.2062												
1	21.09360	0.20854	15.37623	15.53114	30.90737	30.90737	3.82629	3.86484	7.69113	8.00000	8.00000	11.54994	11.66630	0.24884
2	21.59234	0.21091	15.55330	15.70771	31.26101	62.16838	3.90402	3.94278	7.84680	8.00000	8.00000	11.64927	11.76493	0.25101
3	22.09463	0.21327	15.72988	15.88313	31.61301	93.78139	3.98262	4.02143	8.00405	8.00000	8.00000	11.74725	11.86170	0.25319
4	22.60182	0.21562	15.90548	16.05818	31.96366	125.74505	4.06137	4.10036	8.16174	8.00000	8.00000	11.84411	11.95781	0.25534
5	23.11356	0.21796	16.08058	16.23258	32.31316	158.05820	4.13977	4.17890	8.31868	8.00000	8.00000	11.94081	12.05367	0.25744
6	23.63087	0.22029	16.25508	16.40681	32.66189	190.72009	4.21954	4.25893	8.47846	8.00000	8.00000	12.03554	12.14789	0.25958
7	24.15320	0.22263	16.42929	16.58055	33.00985	223.72994	4.29998	4.33957	8.63955	8.00000	8.00000	12.12931	12.24099	0.26173
8	24.68110	0.22495	16.60308	16.75409	33.35717	257.08711	4.38061	4.42045	8.80106	8.00000	8.00000	12.22247	12.33364	0.26384
9	25.21203	0.22727	16.77655	16.92633	33.70288	290.78999	4.46197	4.50180	8.96377	8.00000	8.00000	12.31458	12.42453	0.26596
10	25.74703	0.22957	16.94897	17.09795	34.04692	324.83691	4.54354	4.58348	9.12701	8.00000	8.00000	12.40543	12.51447	0.26807
11	26.28706	0.23187	17.12069	17.26925	34.38993	359.22684	4.62478	4.66491	9.28969	8.00000	8.00000	12.49591	12.60434	0.27013
12	26.83180	0.23416	17.29200	17.44003	34.73203	393.95886	4.70681	4.74710	9.45390	8.00000	8.00000	12.58519	12.69293	0.27220
13	27.38110	0.23644	17.46281	17.61026	35.07307	429.03194	4.78988	4.83033	9.62021	8.00000	8.00000	12.67293	12.77994	0.27429
14	27.93554	0.23872	17.63310	17.78020	35.41330	464.44524	4.87288	4.91354	9.78642	8.00000	8.00000	12.76021	12.86667	0.27635
15	28.49334	0.24099	17.80300	17.94913	35.75212	500.19736	4.95642	4.99710	9.95352	8.00000	8.00000	12.84658	12.95202	0.27840
16	29.05440	0.24325	17.97201	18.11715	36.08916	536.28652	5.04035	5.08105	10.12140	8.00000	8.00000	12.93166	13.03610	0.28046
17	29.62012	0.24550	18.14017	18.28483	36.42499	572.71151	5.12391	5.16477	10.28868	8.00000	8.00000	13.01626	13.12006	0.28246
18	30.19039	0.24774	18.30786	18.45201	36.75987	609.47139	5.20760	5.24860	10.45621	8.00000	8.00000	13.10026	13.20341	0.28445
19	30.76489	0.24997	18.47506	18.61861	37.09367	646.56505	5.29290	5.33403	10.62693	8.00000	8.00000	13.18216	13.28458	0.28649
20	31.34409	0.25220	18.64170	18.78481	37.42651	683.99156	5.37786	5.41915	10.79701	8.00000	8.00000	13.26384	13.36567	0.28849
21	31.92703	0.25442	18.80789	18.95026	37.75815	721.74971	5.46316	5.50451	10.96767	8.00000	8.00000	13.34473	13.44575	0.29047
22	32.51239	0.25663	18.97335	19.11457	38.08792	759.83763	5.54905	5.59036	11.13941	8.00000	8.00000	13.42430	13.52422	0.29247
23	33.10202	0.25883	19.13781	19.27850	38.41631	798.25394	5.63455	5.67597	11.31051	8.00000	8.00000	13.50326	13.60253	0.29442
24	33.69606	0.26102	19.30176	19.44197	38.74373	836.99768	5.71939	5.76094	11.48033	8.00000	8.00000	13.58237	13.68103	0.29631
25	34.29402	0.26321	19.46523	19.60482	39.07005	876.06773	5.80652	5.84816	11.65468	8.00000	8.00000	13.65871	13.75666	0.29830
26	34.89552	0.26538	19.62810	19.76696	39.39505	915.46278	5.89289	5.93458	11.82748	8.00000	8.00000	13.73520	13.83237	0.30023
27	35.49961	0.26755	19.79025	19.92811	39.71836	955.18114	5.97990	6.02156	12.00146	8.00000	8.00000	13.81035	13.90656	0.30216
28	36.10743	0.26970	19.95150	20.08874	40.04024	995.22137	6.06657	6.10830	12.17487	8.00000	8.00000	13.88493	13.98044	0.30407
29	36.71875	0.27185	20.11214	20.24869	40.36083	1035.58220	6.15240	6.19417	12.34657	8.00000	8.00000	13.95974	14.05452	0.30590
30	37.33474	0.27399	20.27215	20.40836	40.68052	1076.26272	6.24016	6.28208	12.52224	8.00000	8.00000	14.03200	14.12628	0.30782
31	37.95444	0.27613	20.43179	20.56740	40.99919	1117.26191	6.32788	6.36987	12.69775	8.00000	8.00000	14.10392	14.19753	0.30971
32	38.57770	0.27825	20.59084	20.72582	41.31665	1158.57857	6.41500	6.45705	12.87205	8.00000	8.00000	14.17584	14.26876	0.31155
33	39.20294	0.28036	20.74923	20.88314	41.63237	1200.21093	6.50330	6.54527	13.04857	8.00000	8.00000	14.24593	14.33787	0.31342
34	39.83172	0.28247	20.90665	21.03996	41.94661	1242.15754	6.59086	6.63288	13.22374	8.00000	8.00000	14.31580	14.40708	0.31525
35	40.46348	0.28456	21.06347	21.19602	42.25949	1284.41703	6.67790	6.71992	13.39782	8.00000	8.00000	14.38557	14.47610	0.31704

Table 9   Rearranged results of the 40 MeV linac calculated by PARMILA.

40 MEV LINAC DESIGN FOR CONSTRUCTION

CELL NUMBER	KINETIC ENERGY	BETA	STEM LENGTH IN CM	TOTAL LENGTH IN CM	TUBE LENGTH IN CM
	20.6000	0.2062			11.5499
1	21.0936	0.2085	30.8989	30.8989	23.3156
2	21.5923	0.2109	31.2607	62.1595	23.5122
3	22.0946	0.2133	31.6130	93.7726	23.7058
4	22.6018	0.2156	31.9640	125.7365	23.8986
5	23.1136	0.2180	32.3126	158.0491	24.0892
6	23.6309	0.2203	32.6617	190.7108	24.2772
7	24.1532	0.2226	33.0099	223.7207	24.4635
8	24.6811	0.2250	33.3569	257.0776	24.6482
9	25.2120	0.2273	33.7029	290.7804	24.8300
10	25.7470	0.2296	34.0472	324.8276	25.0104
11	26.2871	0.2319	34.3896	359.2173	25.1895
12	26.8318	0.2342	34.7316	393.9489	25.3659
13	27.3811	0.2364	35.0732	429.0221	25.5401
14	27.9355	0.2387	35.4131	464.4352	25.7132
15	28.4933	0.2410	35.7520	500.1872	25.8837
16	29.0544	0.2432	36.0894	536.2766	26.0524
17	29.6201	0.2455	36.4250	572.7016	26.2203
18	30.1904	0.2477	36.7591	609.4608	26.3856
19	30.7649	0.2500	37.0939	646.5547	26.5484
20	31.3441	0.2522	37.4264	683.9811	26.7104
21	31.9270	0.2544	37.7579	721.7390	26.8700
22	32.5124	0.2566	38.0882	759.8272	27.0275
23	33.1020	0.2588	38.4167	798.2439	27.1849
24	33.6961	0.2610	38.7426	836.9865	27.3397
25	34.2940	0.2632	39.0705	876.0570	27.4919
26	34.8955	0.2654	39.3948	915.4518	27.6427
27	35.4996	0.2675	39.7186	955.1703	27.7915
28	36.1074	0.2697	40.0407	995.2110	27.9402
29	36.7187	0.2718	40.3599	1035.5709	28.0865
30	37.3347	0.2740	40.6806	1076.2515	28.2302
31	37.9544	0.2761	40.9995	1117.2511	28.3734
32	38.5777	0.2783	41.3161	1158.5671	28.5147
33	39.2029	0.2804	41.6327	1200.1999	28.6537
34	39.8317	0.2825	41.9469	1242.1468	28.7926
35	40.4635	0.2846	42.2702	1284.4170	14.4761

Table 10   Geometry of the new linac

Total length	1284.417	cm
Diameter	90	
Sub-tank length		
No. 7*	307.759	
No. 8	320.208	
No. 9	307.307	
No.10	349.143	
D.T. diameter	16	
Corner radius	4	
Nose radius	0.5	
Bore radius	1.5	
Stem diameter	3.6	
Post diameter	3.0	
stroke	16	
Tab major axis	6.6	
minor axis	3.8	
thickness	2	
rotation angle	180°	
Frequency tuner		
diameter	12.5	
stroke	18	
Auto-frequency tuner		
diameter	11.5	
stroke	12	

* Tank numbers from 1 to 6 are named the old sub-tanks.

Table 11

Resonant frequencies and Q values of DT-less sub-tank

Tank number	No.7	No.8	No.9	No.10
Measured frequency	254.911	254.902	254.901	254.898
Calculated frequency	254.995	254.995	254.976	254.987
Deviation (%)	- 0.036	- 0.039	- 0.039	- 0.041
Length (mm)	3077.59	3202.08	3073.07	3491.43
Diameter (mm)	900.02	900.02	900.09	900.05
Design diameter	900.00			
Design frequency	255.002			
Q value	73000	75000	73000	75000
Calculated Q value	95850	96330	95840	97330

Table 12

Resonant frequencies and Q values of
sub-tanks with drift tubes

tank number	frequency	Q value
No.7	200.804	54000
No.8	200.870	55000
No.9	200.816	57000
No.10	200.745	59000

Table 13

Insertion length of frequency tuners to make a
nearly flat field distribution

Tuner number	length (mm)
1	106
2	112
3	118
4	58
5	64
6	70
7	132
8	138
9	144
10	150
11	156
12	162
auto-1	47
auto-2	47

Table 14   Tab rotation during fine tuning

Tab number	rotation angle (degree)	
2	down	10
3	down	15
18	down	25
28	up	14
31	up	10

Down means the direction towards the high-energy
  end of the linac.
Up means the direction towards the low-energy
  end of the linac.
Normally, tabs point in the vertical direction.

Table 15   Field distribution and transit-time factor
           of the 40-MeV linac during stabilization

cell number	E	T	T (calculation)
1	0.987	0.878	0.870
2	0.994	0.876	0.869
3	0.996	0.874	0.865
4	0.988	0.874	0.864
5	0.987	0.871	0.863
6	0.991	0.870	0.863
7	0.999	0.867	0.862
8	0.993	0.865	0.862
9	0.996	0.864	0.858
10	0.998	0.861	0.856
11	0.991	0.860	0.855
12	0.988	0.860	0.854
13	0.995	0.857	0.853
14	0.994	0.856	0.853
15	0.993	0.854	0.850
16	0.994	0.853	0.847
17	0.997	0.852	0.846
18	0.997	0.850	0.845
19	0.992	0.847	0.844
20	0.991	0.845	0.843
21	0.993	0.846	0.841
22	0.993	0.844	0.837
23	0.989	0.842	0.836
24	0.992	0.840	0.835
25	0.996	0.840	0.834
26	0.994	0.838	0.832
27	0.999	0.834	0.828
28	1.000	0.832	0.827
29	0.999	0.831	0.825
30	0.998	0.830	0.825
31	0.995	0.830	0.823
32	0.995	0.827	0.822
33	0.993	0.825	0.818
34	0.997	0.823	0.817
35	1.000	0.821	0.814

Table 16

Resonant modes during stabilization
(in the air, 23°C)

TM014	209.34
TM013	206.74
TM012	204.55
TM011	202.61
TM010	201.04
post-1	199.91
post-2	198.90
post-3	198.12
post-4	197.40
post-5	196.96
stem-1	81.09
stem-2	80.8
stem-3	80.56

Table 17

Comparison of calculated and measured frequencies

	Calculation	Measurements[*]
TM010	200.99	200.65
TM011	201.30	200.95
TM012	202.17	201.85
TM013	203.78	203.35
TM014	205.68	205.45

* Contribution of frequency tuners and
post couplers are eliminated
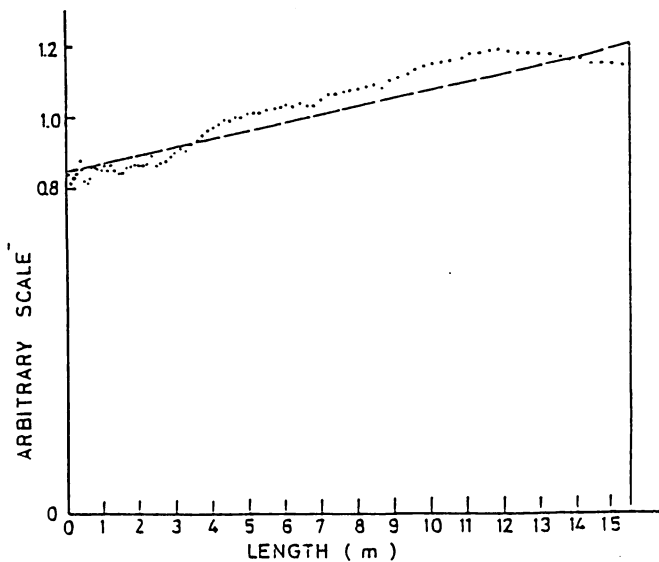
Fig. 1 Average axial electric field of the 20 MeV linac measured in 1974 from reference (14).

axial distance (m)

Fig. 2 Average electric field of the 20 MeV linac measured in 1979 from reference (15).

Fig. 3 Operation records of the Booster magnetic field during beam injection vs. tank level from 1981 to 1983.
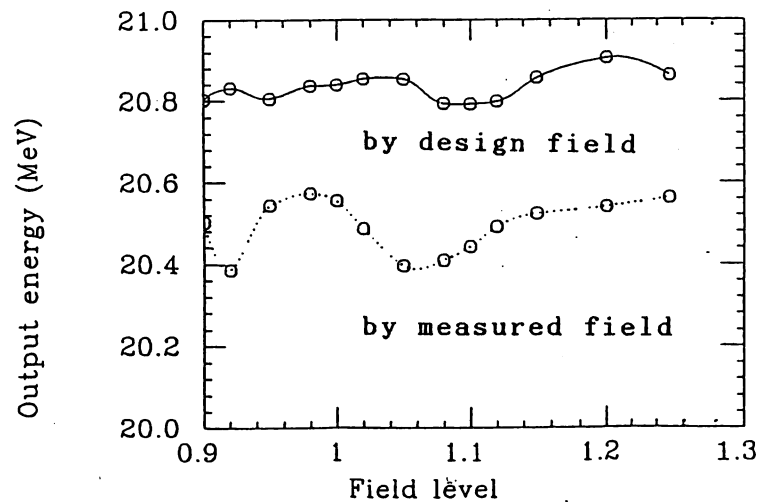
Fig. 4 Calculated average output energy of the 20-MeV linac vs. the field level. The solid curve is based on the design field distribution, while the dashed curve is based on the measured field distribution.
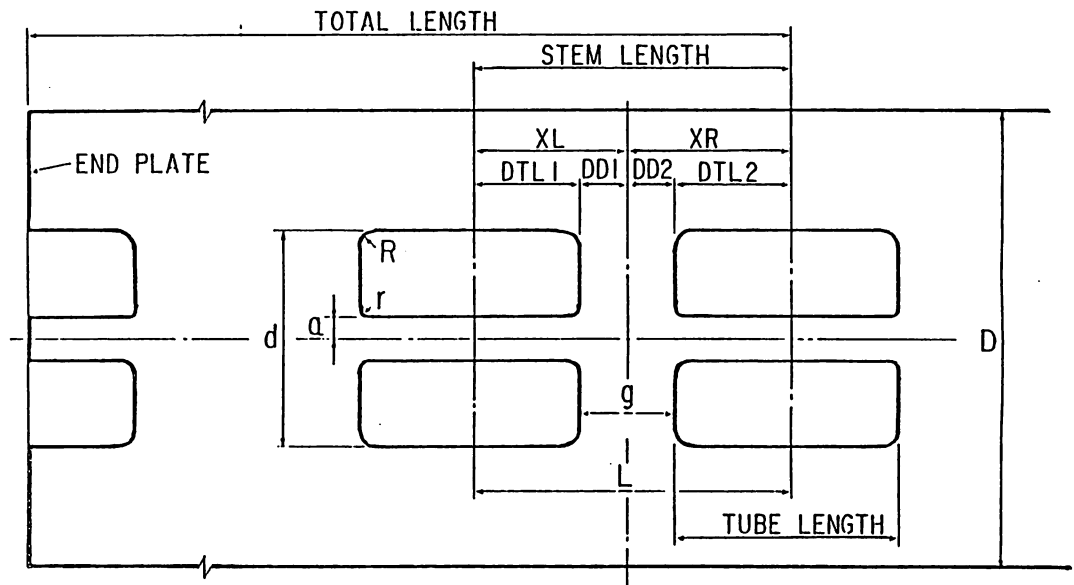
Fig. 5 Geometry of a drift tube linac.
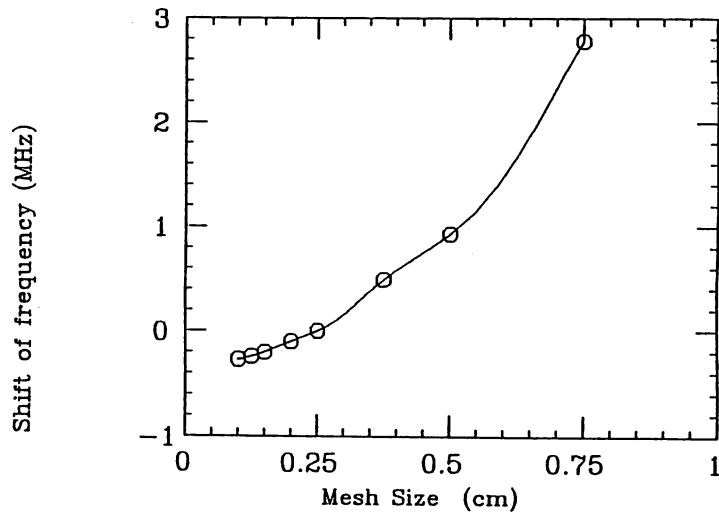
Fig. 6 Mesh size dependence of the SUPERFISH frequency.
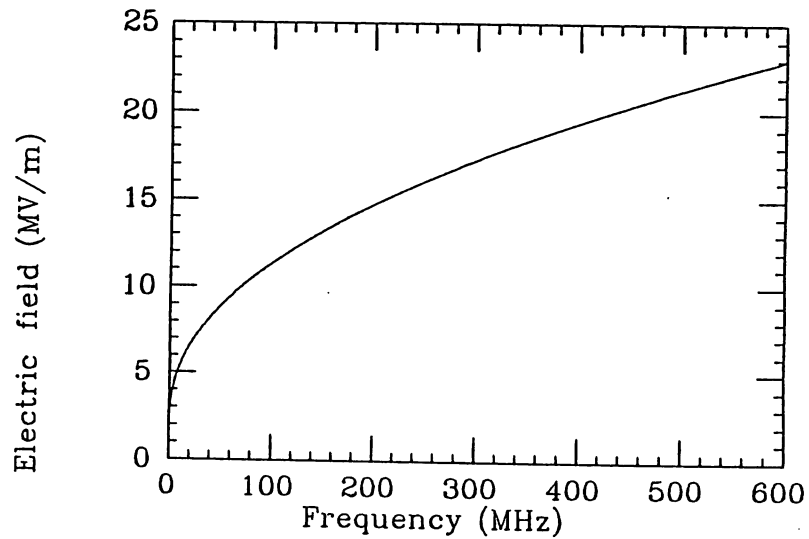
Fig. 7 Kilpatrick field limit vs. rf frequency.
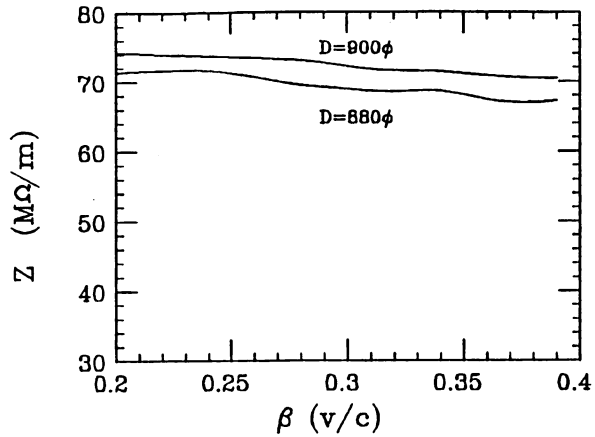
Fig. 8 Shunt impedance vs. β (v/c) for tank diameters of 900 and 880 mm.
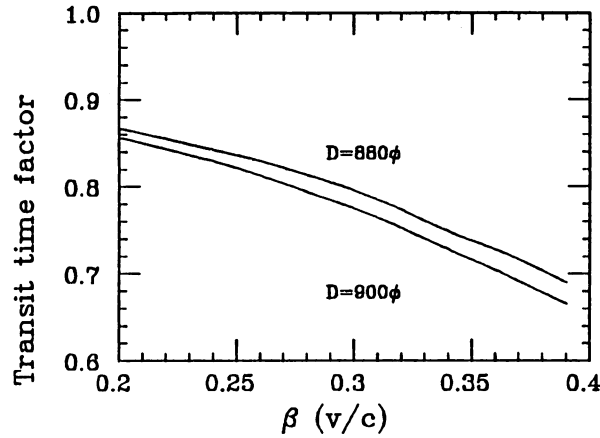
Fig. 9 Transit time factor vs. β for tank diameters of 900 and 880 mm.
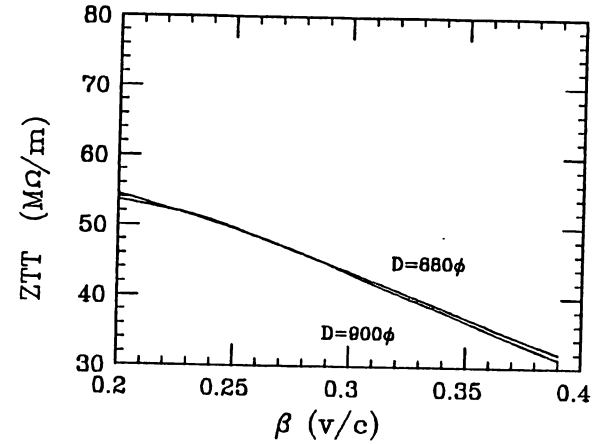
Fig. 10 Effective shunt impedance vs. β for tank diameters of 900 and 880 mm.
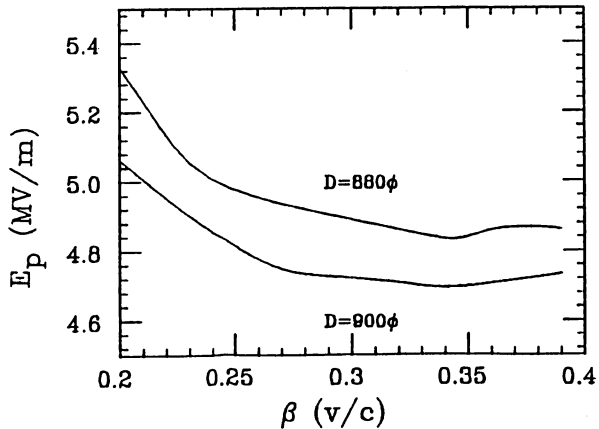
Fig. 11 Maximum surface electric field vs. β for tank diameters of 900 and 880 mm.
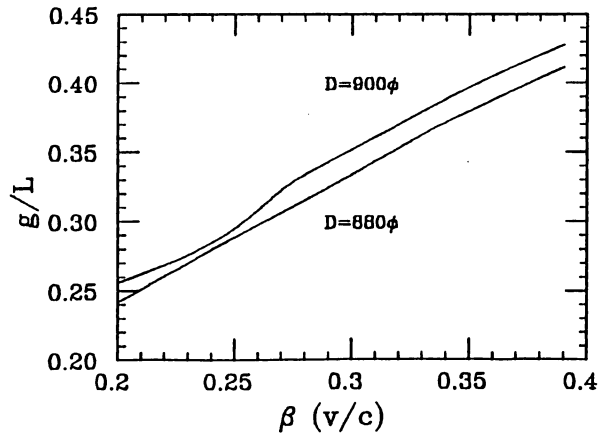
Fig. 12 g/L vs. β for tank diameters of 900 and 880 mm.
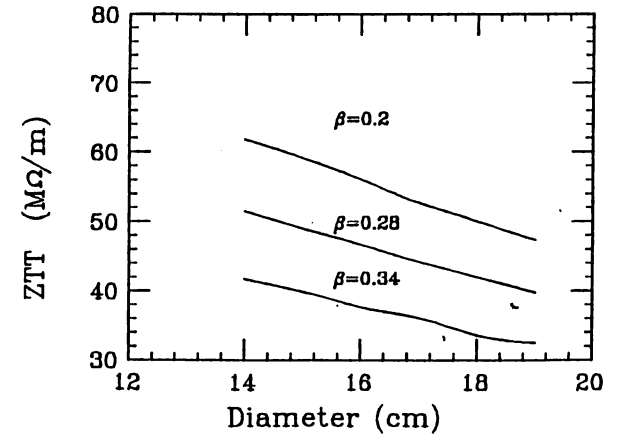
Fig. 13 Effective shunt impedance vs. diameter of the drift tube.
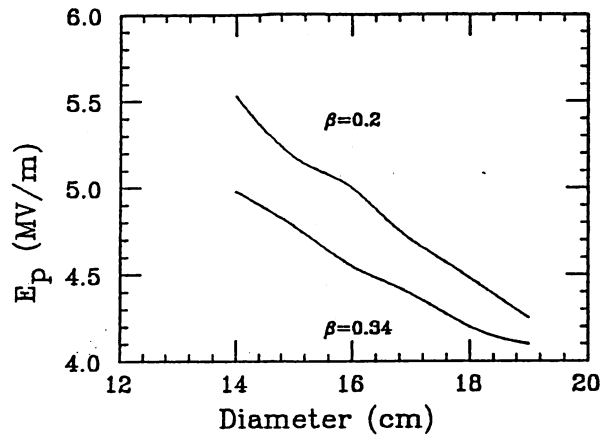
Fig. 14 Maximum surface electric field vs. the diameter of the drift tube.
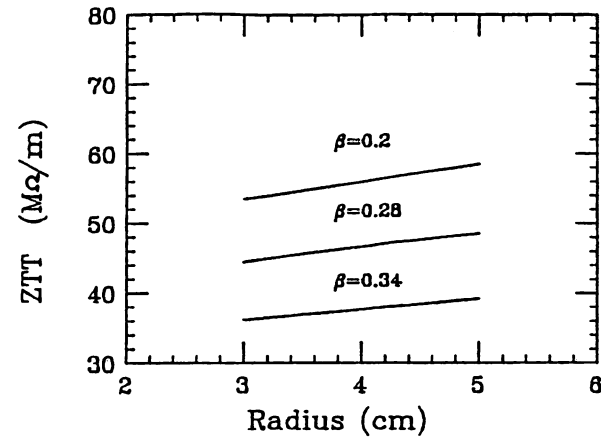
Fig. 15 Effective shunt impedance vs. the corner radius.
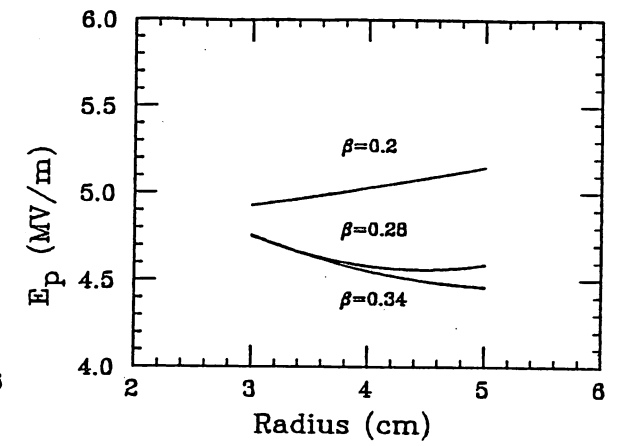
Fig. 16 Maximum surface electric field vs. the corner radius.
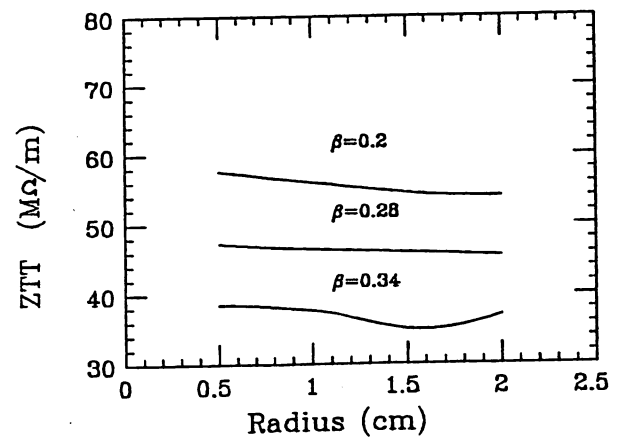
Fig. 17 Effective shunt impedance vs. nose radius.
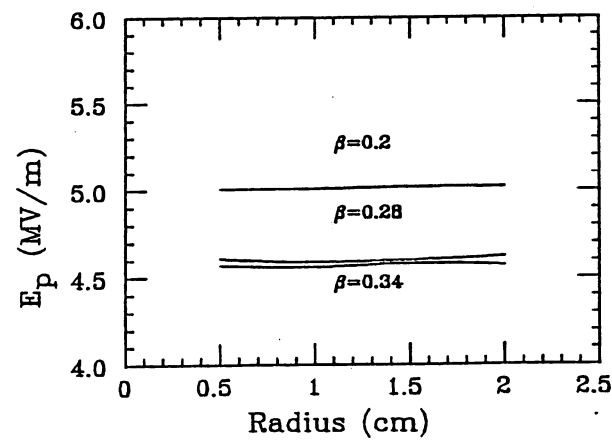
Fig. 18 Maximum surface electric field vs. corner radius.
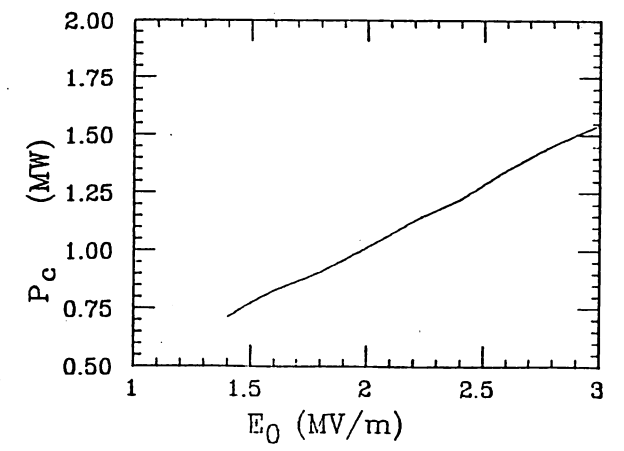
Fig. 19 Required rf power vs. field strength.
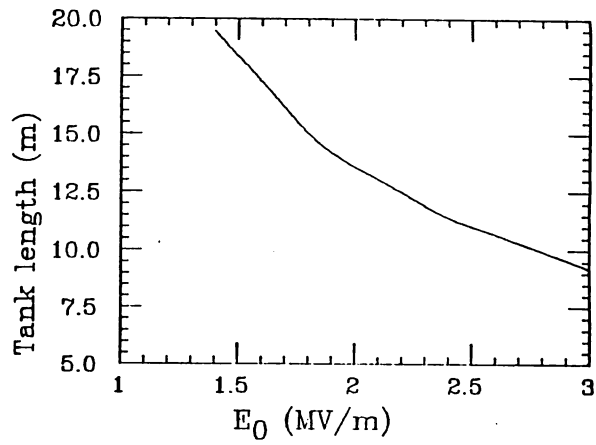
Fig. 20   Required tank length vs. field
          strength.
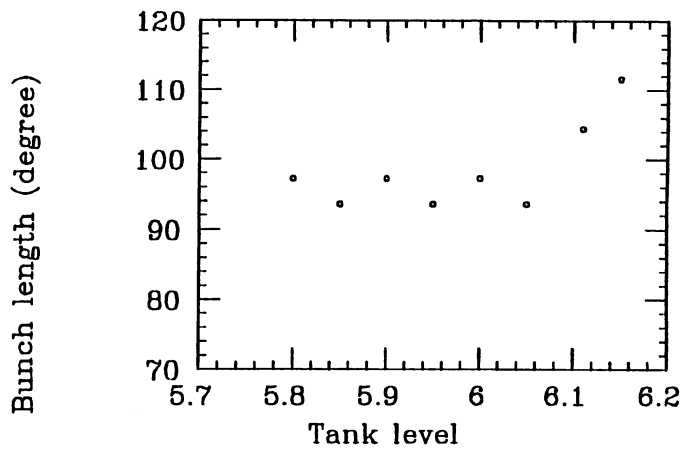
Fig. 21   Measured bunch length of the 20
          MeV linac vs. relative field
          level, i.e., tank level.
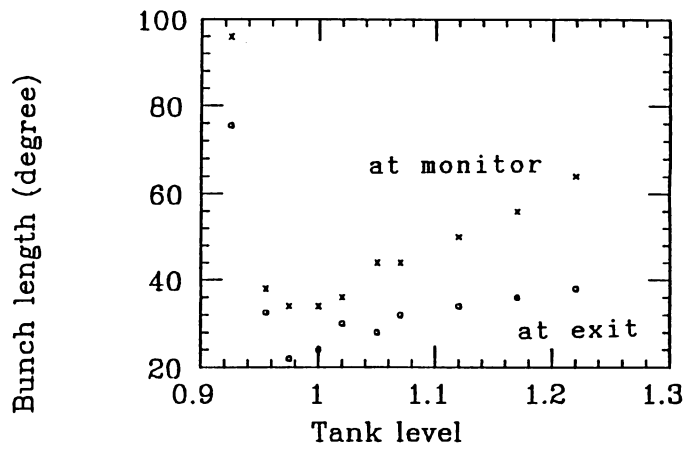
Fig. 22   Calculated bunch length on the
          basis of the measured field
          distribution vs. field level.
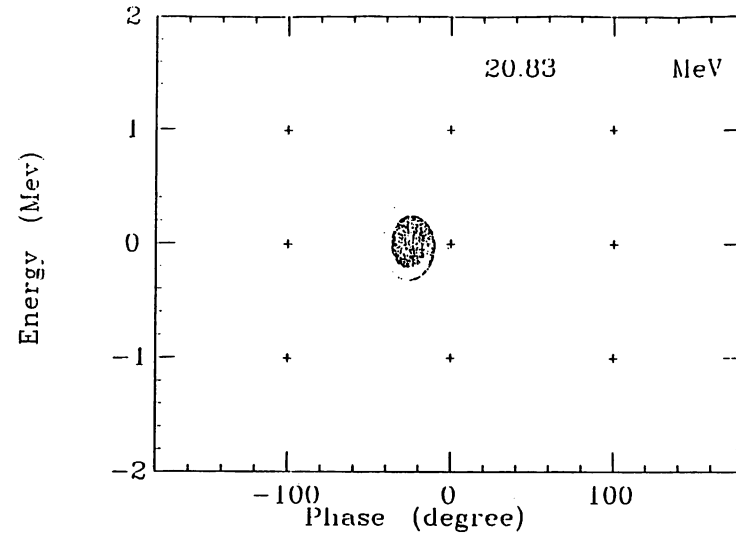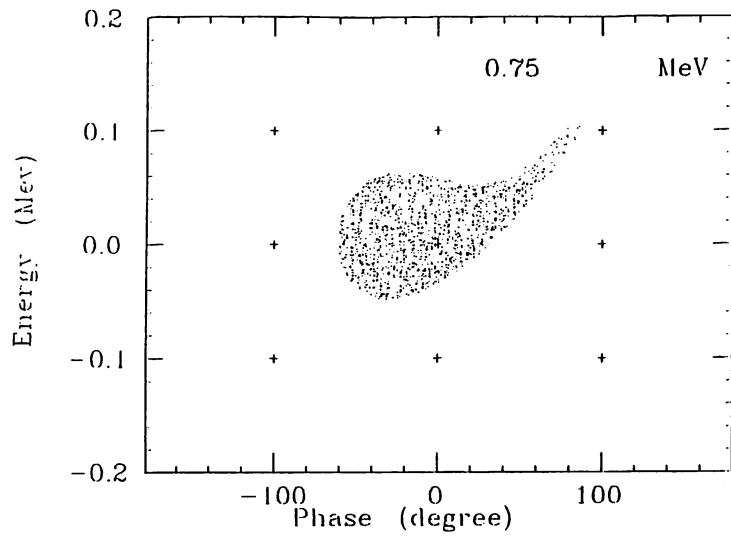
a) 20 MeV entrance.

b) 20 MeV exit.
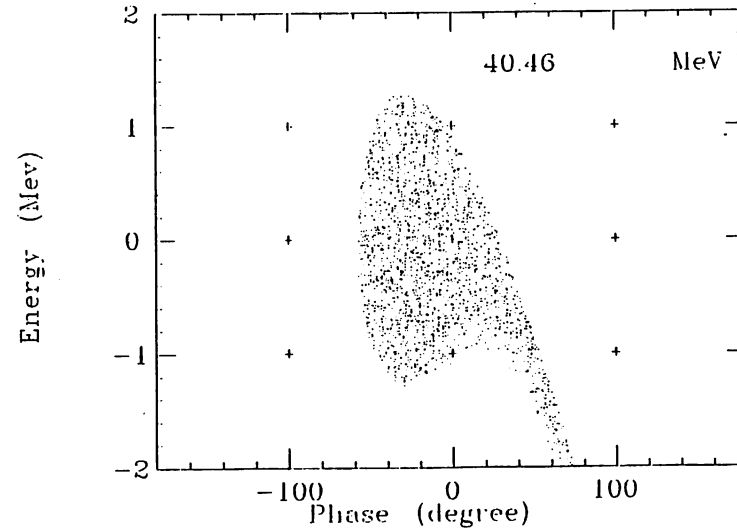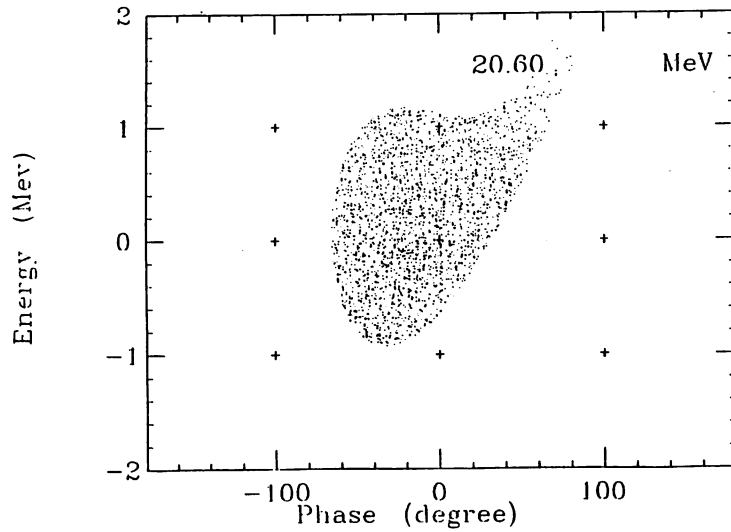
c) 40 MeV entrance.

d) 40 MeV exit.

Fig. 23 Calculated longitudinal acceptance of the 20- and 40-MeV Linacs.
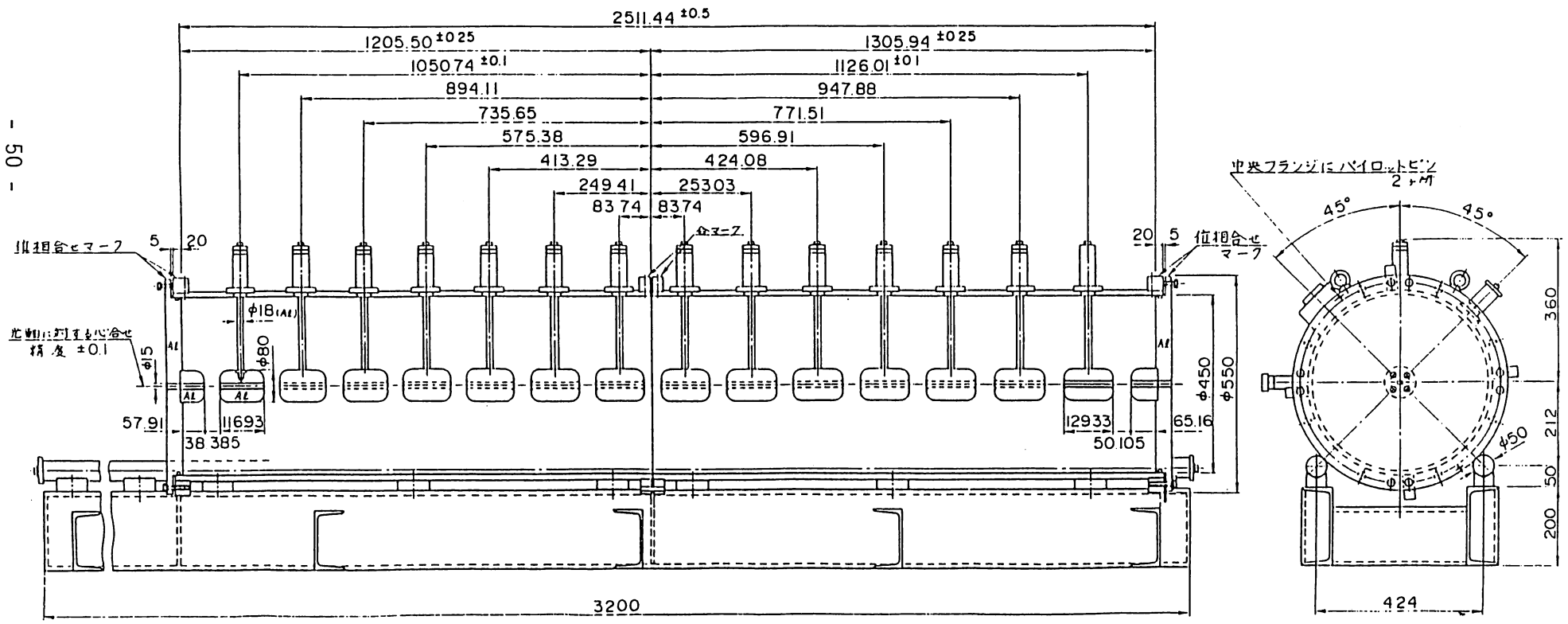
Fig. 24 Geometry of the model linac.
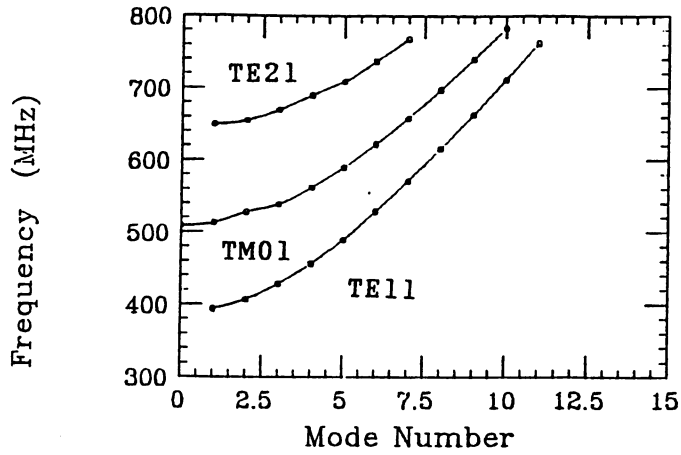
Fig. 25 Measured resonant modes of the cylindrical model linac without drift tubes.
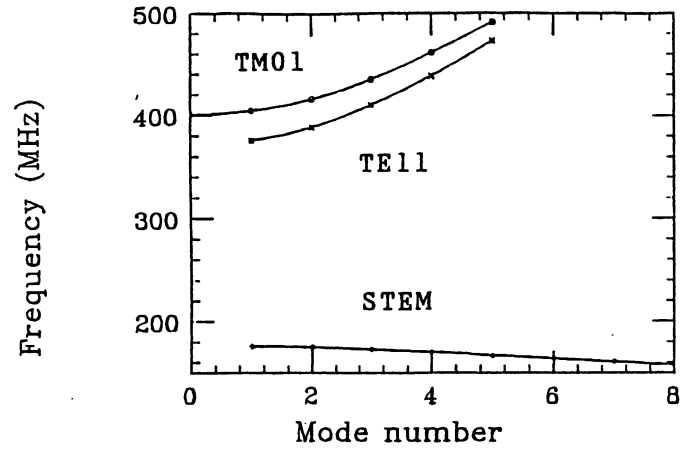
Fig. 26 Measured dispersion relation of the post-less model linac.
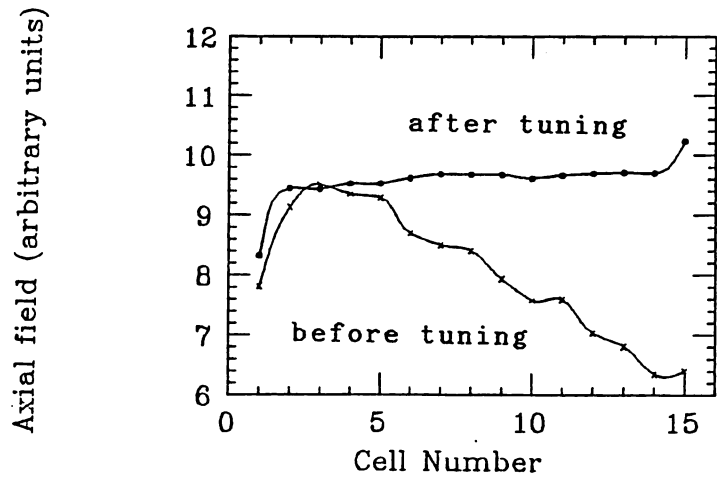
Fig. 28 Field distribution of the model linac during post tuning.
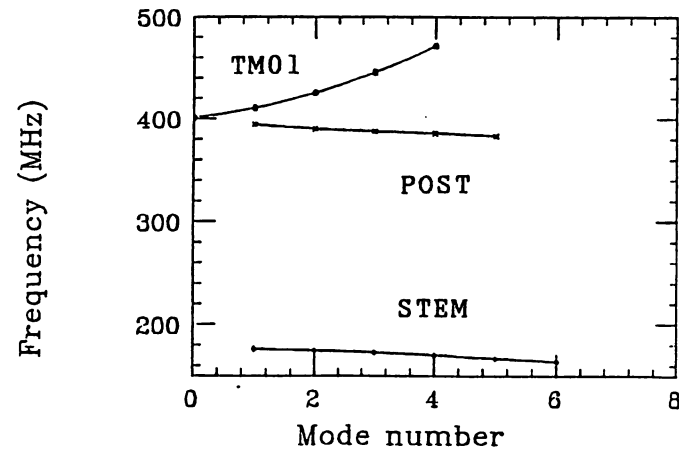
Fig. 29 Measured dispersion relation during stabilization.
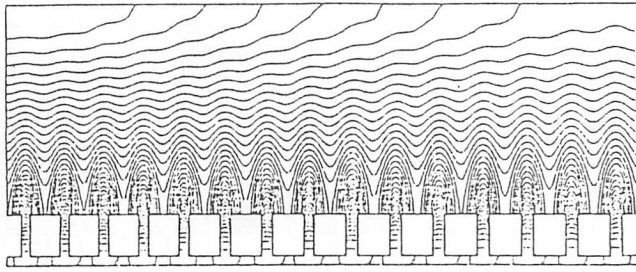
TM010   401.895 MHz
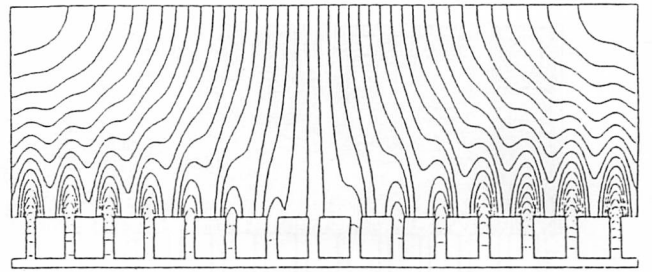
TM011   406.245 MHz
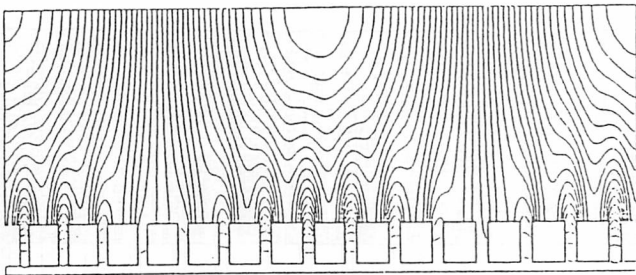
TM012   418.929 MHz
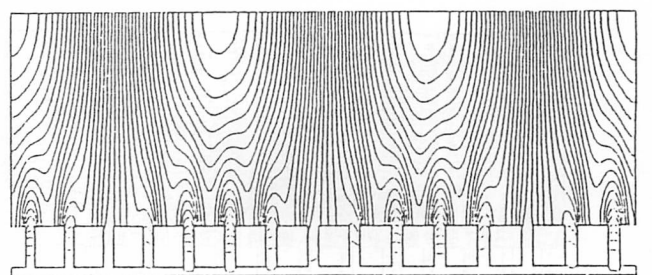
TM013   439.272 MHz
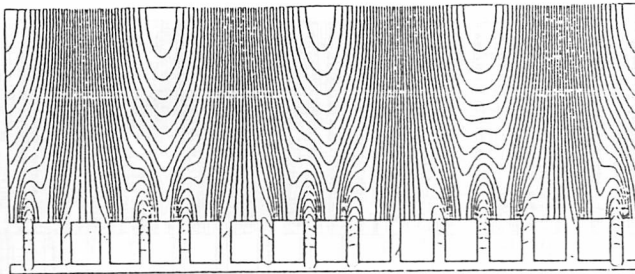
TM014   466.302 MHz
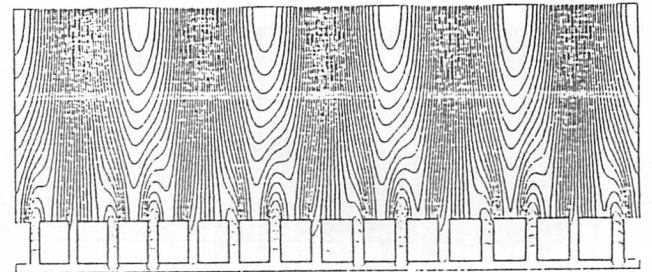
TM015   498.779 MHz
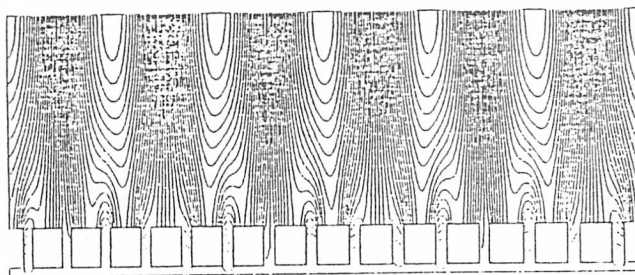
TM016   535.838 MHz
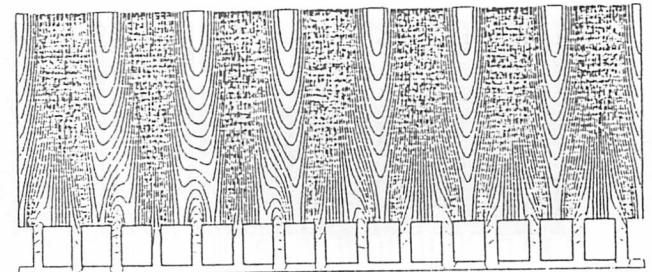
TM017   576.419 MHz

Fig. 27 Calculated TM01n modes of the 15-cell model linac by SUPERFISH.
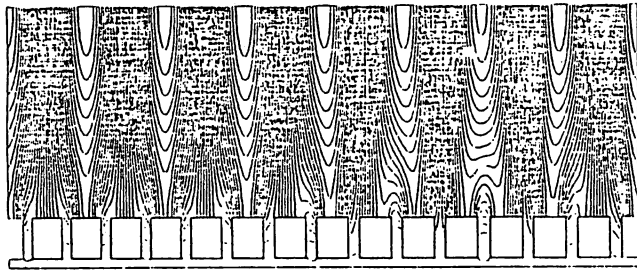
TM018   619.863 MHz
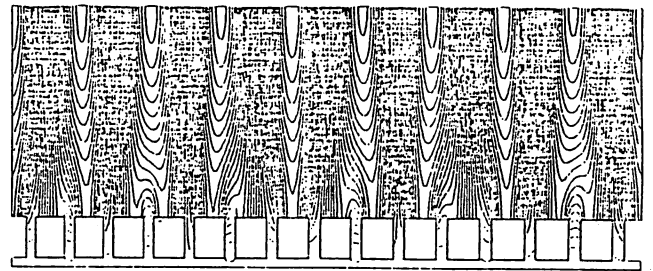
TM019   665.443 MHz
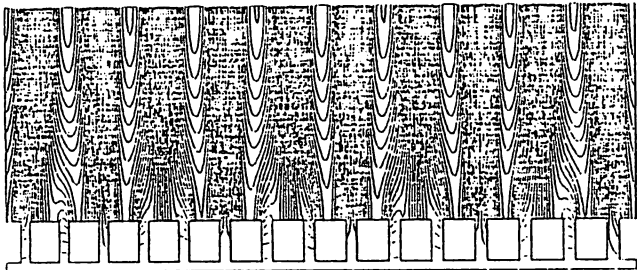
TM0110   712.632 MHz
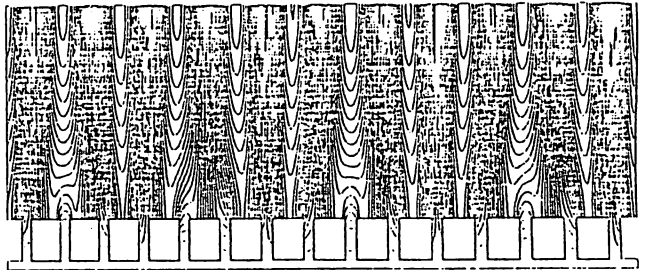
TM0111   760.797 MHz
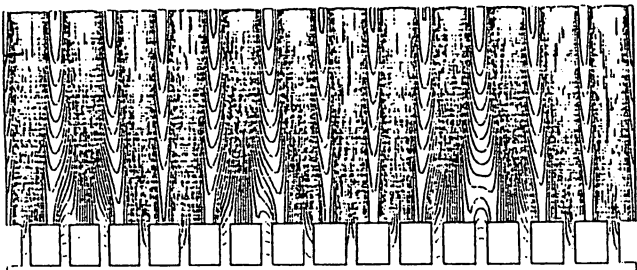
TM0112   808.903 MHz
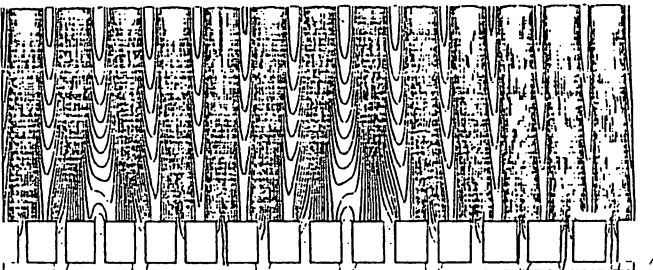
TM0113   853.426 MHz
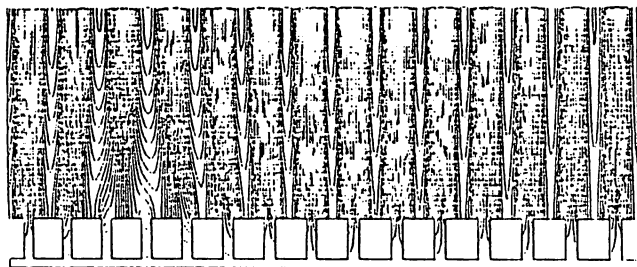
TM0114   890.638 MHz
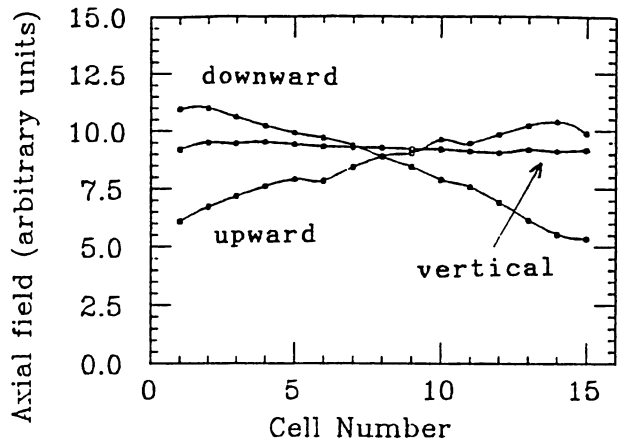
Fig. 30 Effect of tab rotation on the field distribution of the model linac.
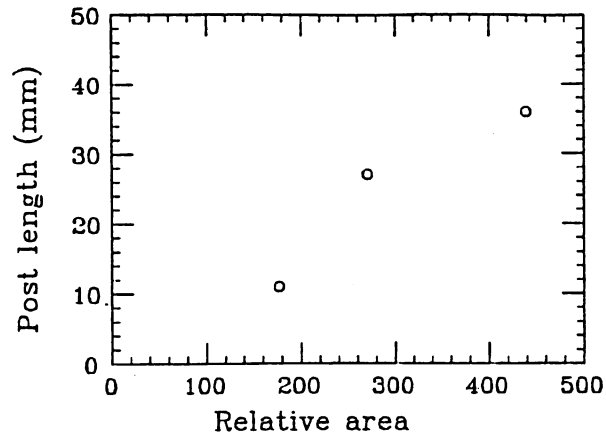
Fig. 31 Post length during stabilization vs. relative tab area. The relative area includes a correction for the length of the post coupler for each measurement.
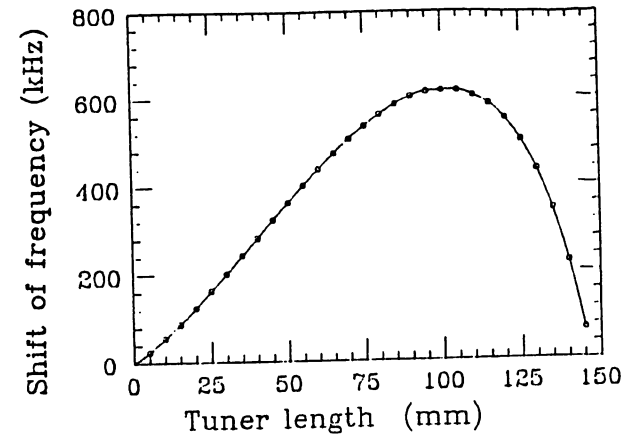
Fig. 32 Shift in the resonant frequency of the model linac by four tuners.
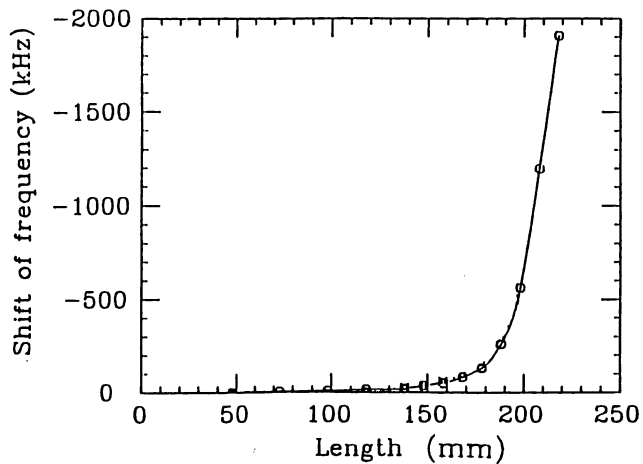
Fig. 33 Shift of the resonant frequency of the model linac by a tuning ball.
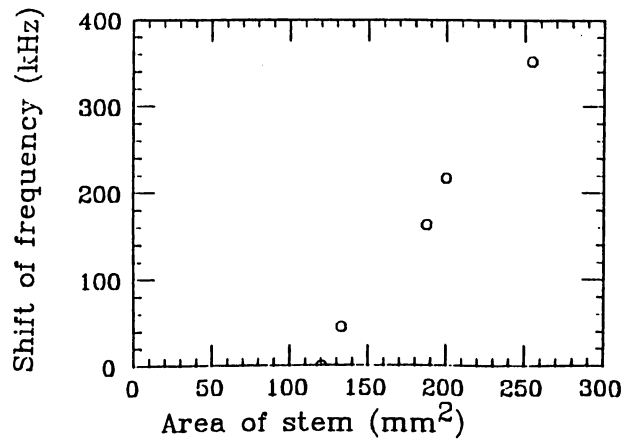
Fig. 34 Effect of stems on the resonant frequency of the model linac.
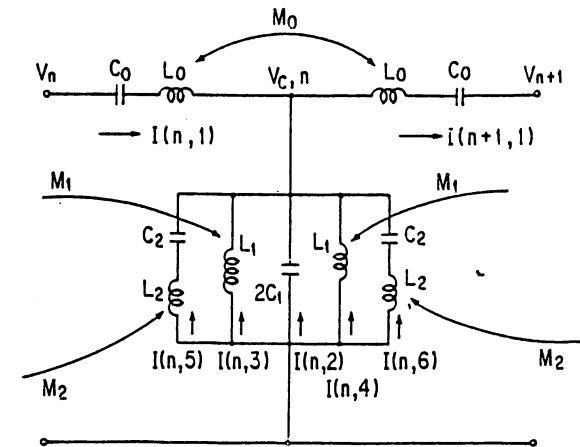
Fig. 35 Equivalent circuit for a post-coupled structure.
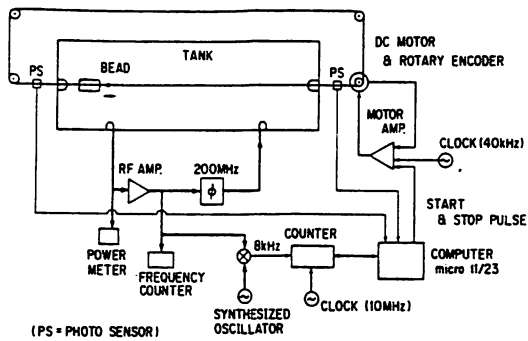
Fig. 36 Block diagram of the field measurement.
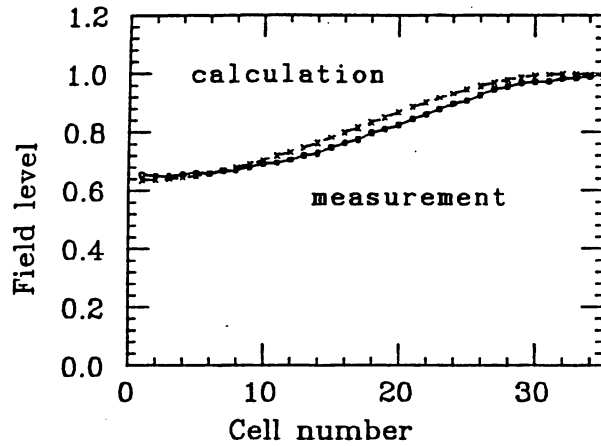
Fig. 37 Measured TM010 field when the post couplers were pulled out exceedingly. $D_x = 0.14$. Dashed curve shows the results of calculation.
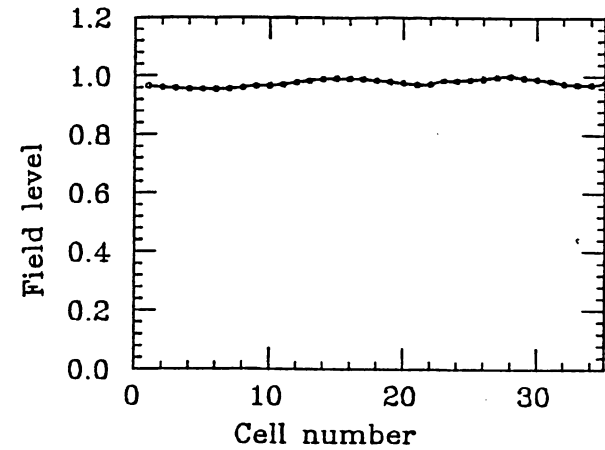
Fig. 38 Measured TM010 field adjusted by 14 frequency tuners. $D_x = 0.0114$.
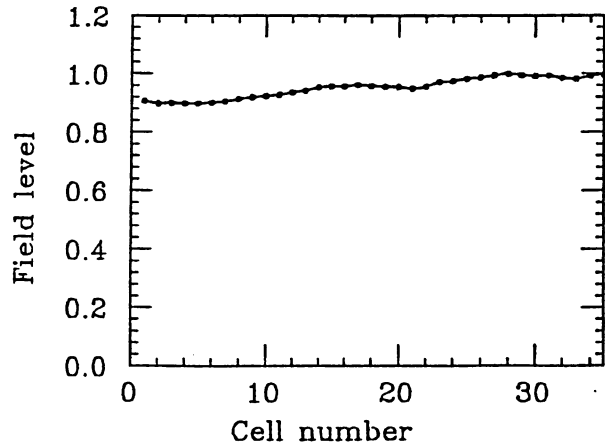
Fig. 39 Measured TM010 field with a 10 % inclined field tilted by both end tuners. $D_x = 0.0306$.
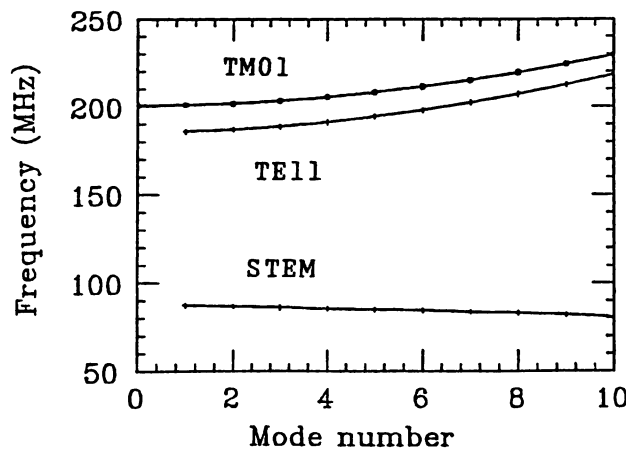
Fig. 40 Measured dispersion relation of the post-less 40 MeV linac.
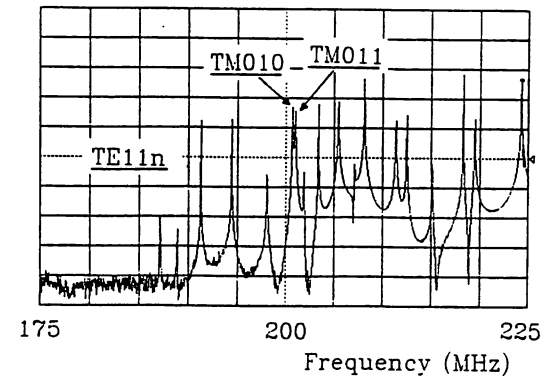
Fig. 41 Measured resonant modes of the post-less 40-MeV linac.
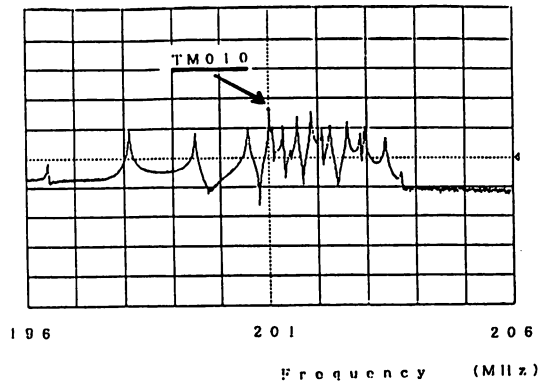
Fig. 42 Measured resonant modes of the 40-MeV linac for a post length = 92 mm.
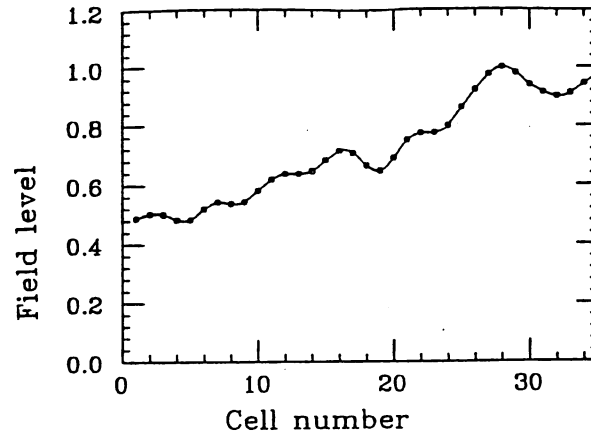
Fig. 43 Measured TM010 field of the 40-MeV linac strongly perturved for a post length = 90 mm. D_x = 0.207.
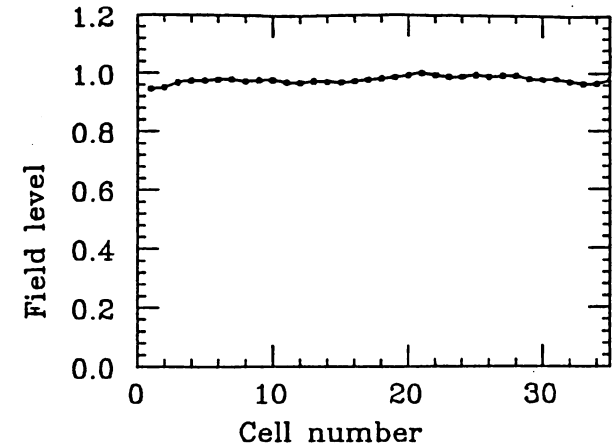
Fig. 44 Measured TM010 field of the 40 MeV linac during stabilization. Post length = 74 mm, D_x = 0.00886.
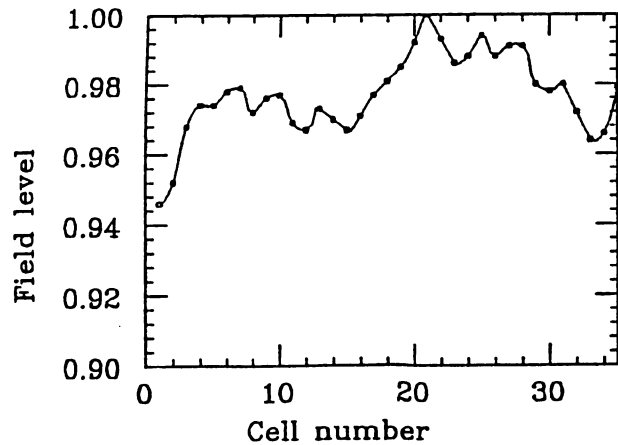
Fig. 45 Measured TM010 field of the 40-MeV linac during stabilization. This is the same as Fig. 44 except for the scale of the ordinate.
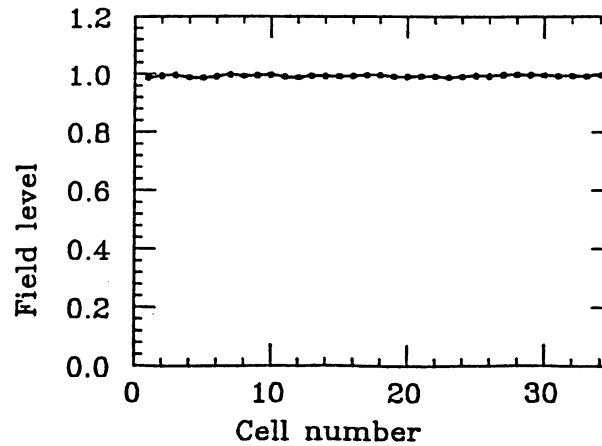
Fig. 46 Measured TM010 field of the 40 MeV linac during stabilization. Tab rotation is used D_x = 0.0029.
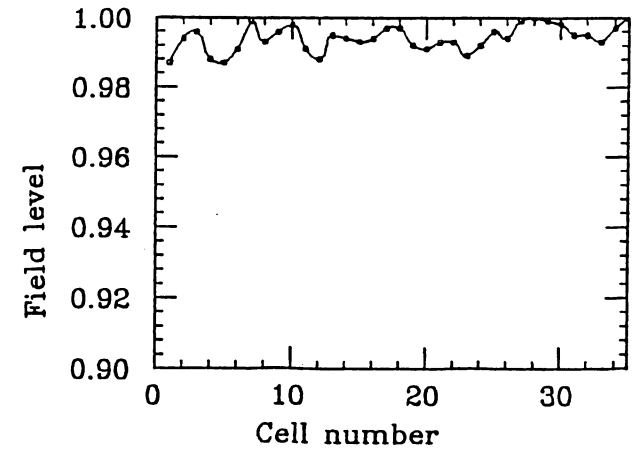
Fig. 47 Measured TM010 field of the 40 MeV linac during stabilization. Tab rotation is used. D_x = 0.0029. This is the same as Fig. 46 except a scale of ordinate.
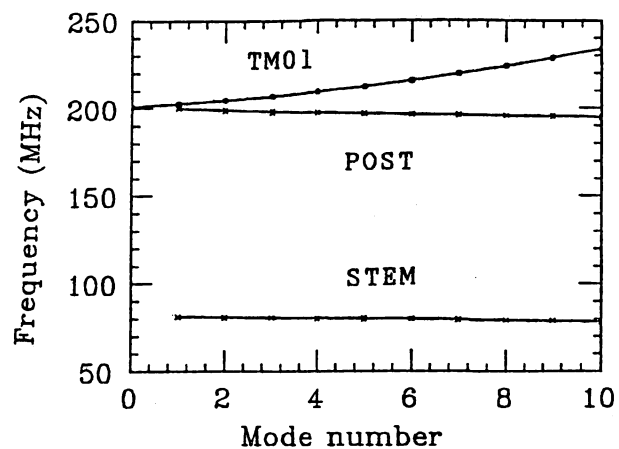
Fig. 48 Measured dispersion relation
         of the 40-MeV linac during
         stabilization.
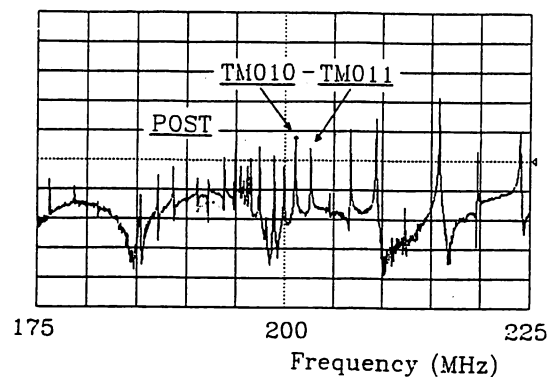
Fig. 49 Measured resonant modes of the
         40-MeV linac during stabilization.
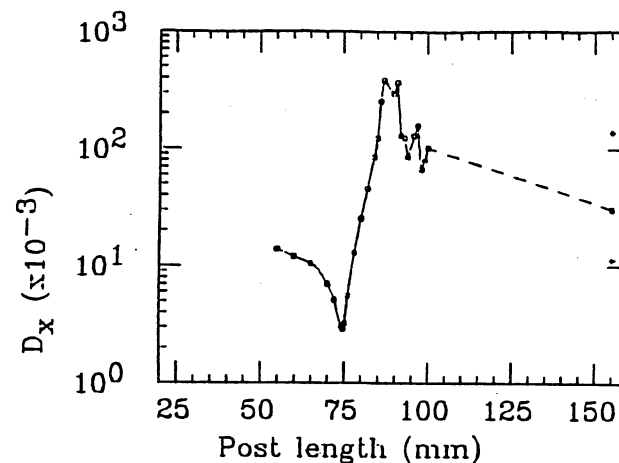
Fig. 50 Measured distortion parameter of
         the 40-MeV linac vs. post length.
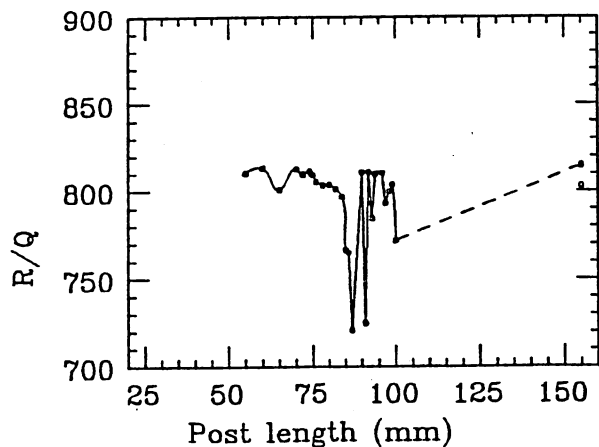
Fig. 51 Measured R/Q of the 40 MeV linac
         vs. post length.
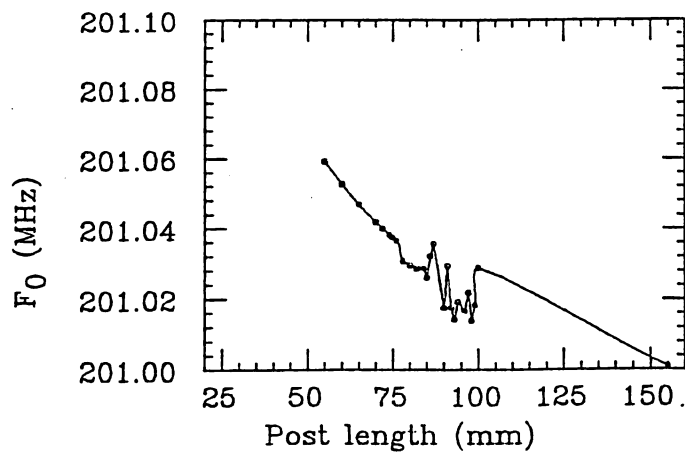
Fig. 52 Measured TM010 resonant frequency
         of the 40-MeV linac vs. post length.
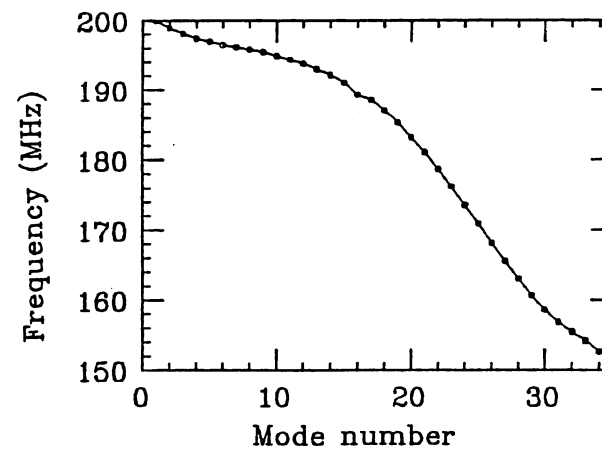
Fig. 53 Measured post modes of the 40 MeV
         linac at the stabilization. Post
         length = 74 mm.

MKR(430):206.725 2MHz 85.09.14 23:46
A(*):MAGTD   -45.72dB 1/128 M0 0.1dB/

CF:206.725 2MHz SPAN:0Hz
STOP:4.00dBm EL:0.00cm
IRG(R):0dBm IRG(T):0dBm 60.0sec RBW:100Hz VBW:100Hz 50a
MAX-HLD OFF AVG ? 128 MEAP ? 1001 BRKP ? 1001

a) TM013

MKR(431):202.642 2MHz 85.09.14 23:42
A(*):MAGTD   -42.18dB 1/128 M0 0.1dB/

CF:202.642 2MHz SPAN:0Hz
STOP:4.00dBm EL:0.00cm
IRG(R):0dBm IRG(T):0dBm 60.0sec RBW:100Hz VBW:100Hz 50a
MAX-HLD OFF AVG ? 128 MEAP ? 1001 BRKP ? 1001

b) TM011

MKR(477):201.024 1MHz 85.09.14 23:40
A(*):MAGTD   -27.73dB 1/128 M0 -27.74dB

CF:201.024 1MHz SPAN:0Hz
STOP:4.00dBm EL:0.00cm
IRG(R):0dBm IRG(T):0dBm 60.0sec RBW:100Hz VBW:100Hz 50a
MAX-HLD OFF AVG ? 128 MEAP ? 1001 BRKP ? 1001

c) TM010

MKR(446):199.919 8MHz 85.09.14 23:49
A(*):MAGTD   -37.18dB 1/128 M0 -37.17dB

CF:199.919 8MHz SPAN:0Hz
STOP:4.00dBm EL:0.00cm
IRG(R):0dBm IRG(T):0dBm 60.0sec RBW:100Hz VBW:100Hz 50a
MAX-HLD OFF AVG ? 128 MEAP ? 1001 BRKP ? 1001

d) post-1

MKR(476):198.887 4MHz 85.09.14 23:52
A(*):MAGTD   -57.10dB M0 -57.14dB

CF:198.887 4MHz SPAN:0Hz
STOP:4.00dBm EL:0.00cm
IRG(R):0dBm IRG(T):0dBm 60.0sec RBW:100Hz VBW:100Hz 50a
MAX-HLD OFF AVG ? 1 MEAP ? 1001 BRKP ? 1001

e) post-2

Fig. 54 Measured rf amplitudes of some resonant modes of the 40-MeV linac by axial-bead perturbation during stabilization.
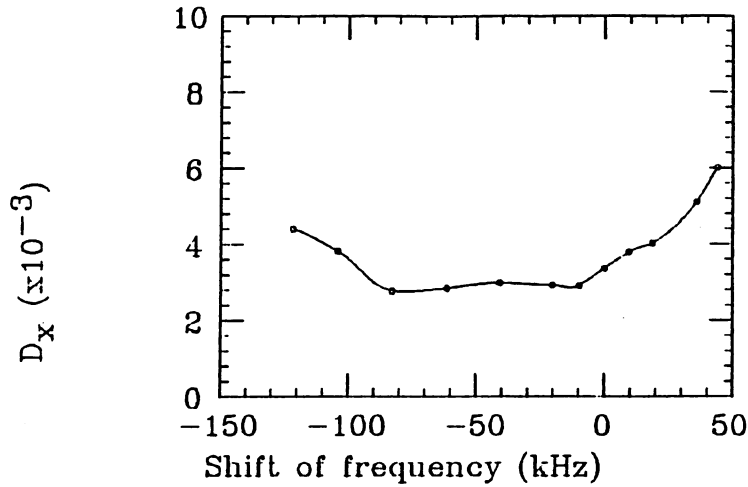
Fig. 55 Variation of the distortion parameters vs. twelve frequency tuners.
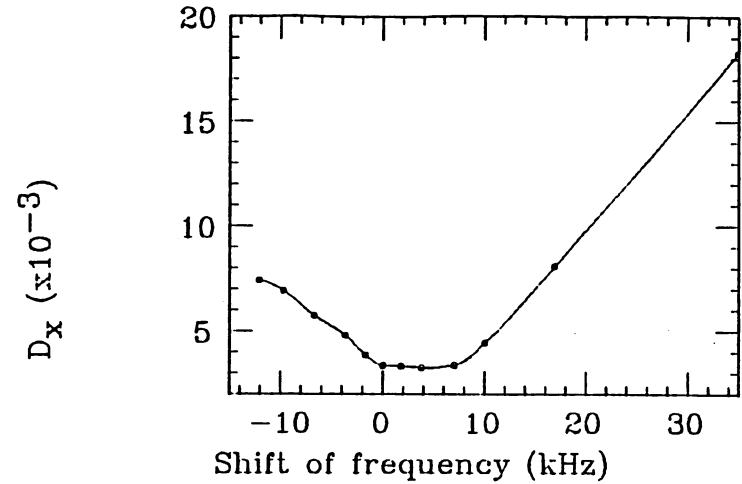
Fig. 56 Variation of the distortion parameter vs. auto-tuners.
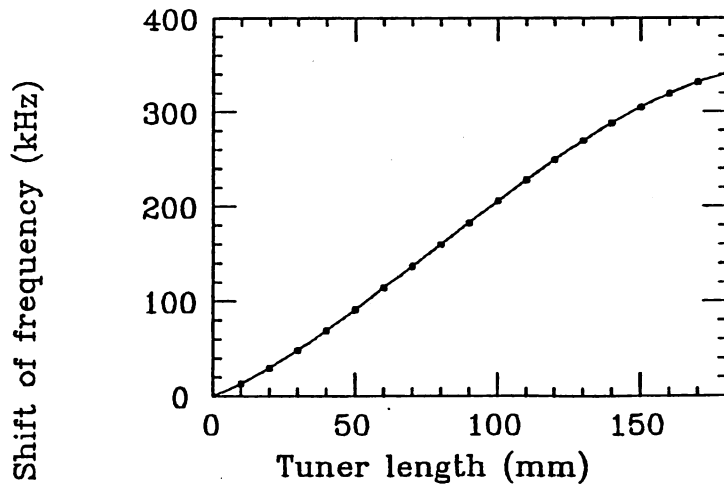
Fig. 57 Shift of the TM010 frequency by twelve frequency tuners.
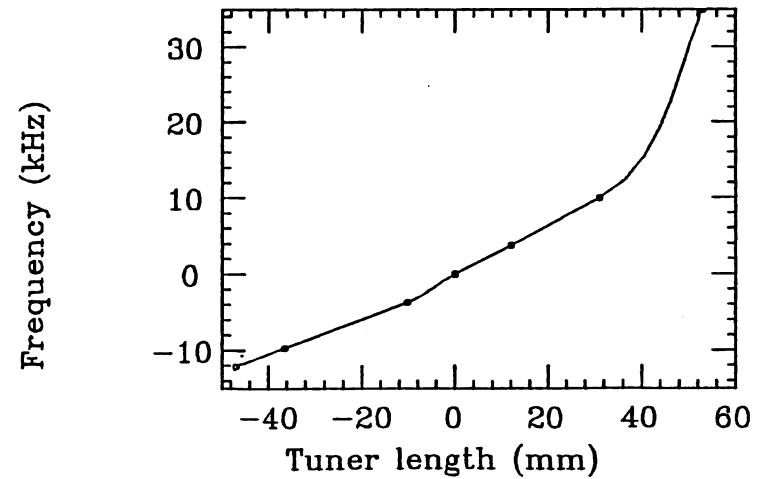
Fig. 58 Shift of the TM010 frequency by auto-tuners.
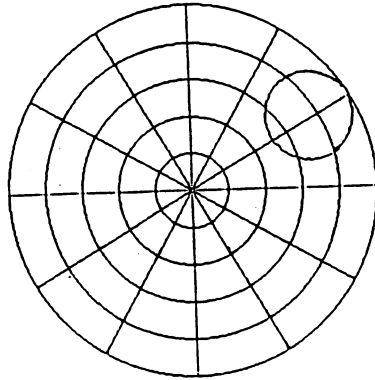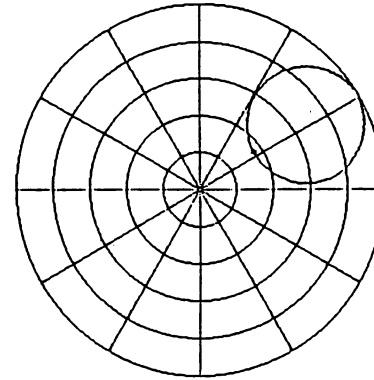
a) View of port-1. Port-2 is terminated
   in a matched load impedance.
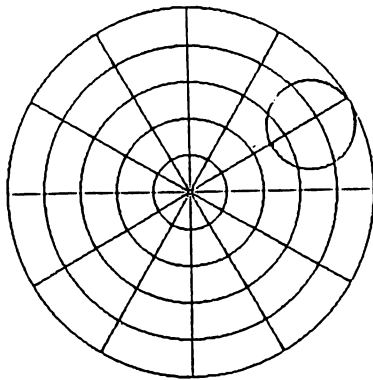
b) View of port-1. Port-2 is terminated
   in a open-circuit termination.

c) View of port-2. Port-1 is terminated
   in a matched load impedance.
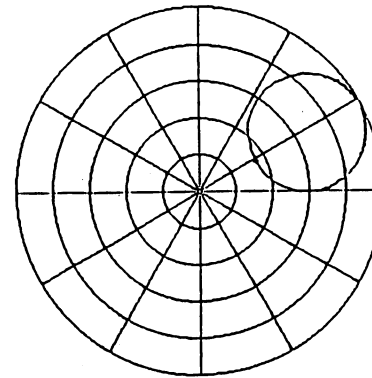
d) View of port-2. Port-1 is terminated
   in a open-circuit termination.

Fig. 59 Polar view of two rf input couplers when
         a matched condition of the couplers are achieved.
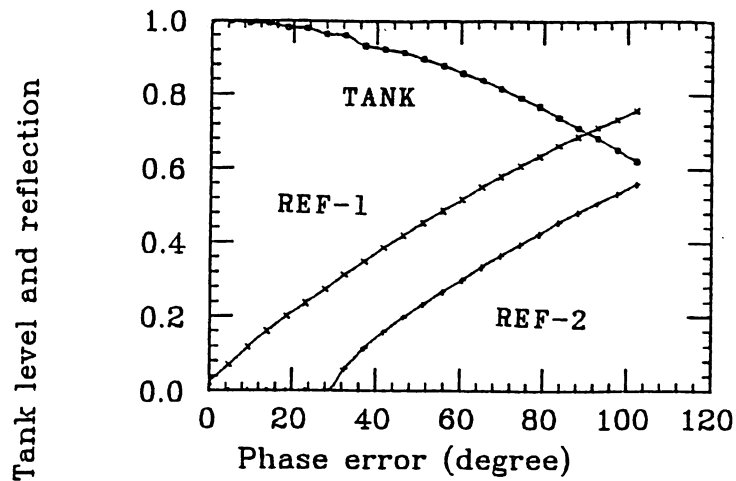
Fig. 60 Measured field amplitude and the voltage reflection coefficients vs. rf input phase shift of one port when a two-feed operation is being peformed.
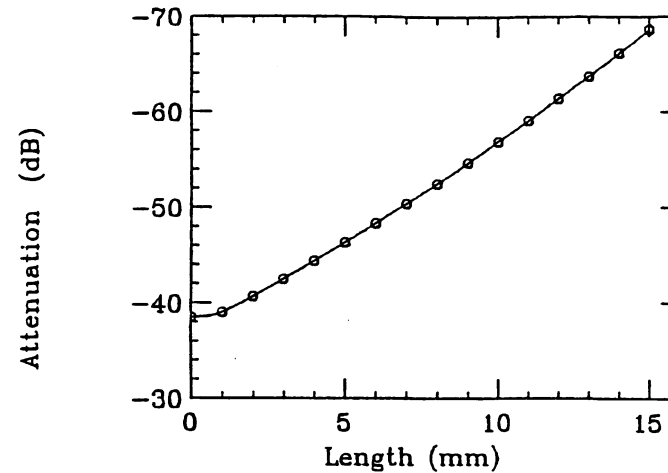
Fig. 61 Measured attenuation of the rf monitor coupler vs. extraction length.
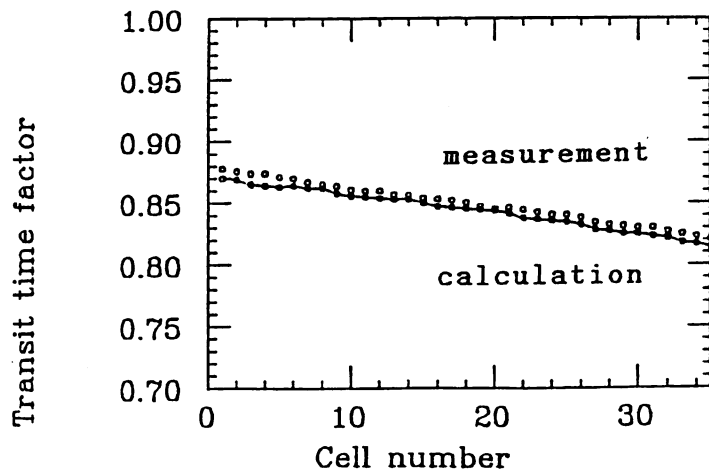
Fig. 62 Measured and calculated transit time factors of the 40 MeV linac.
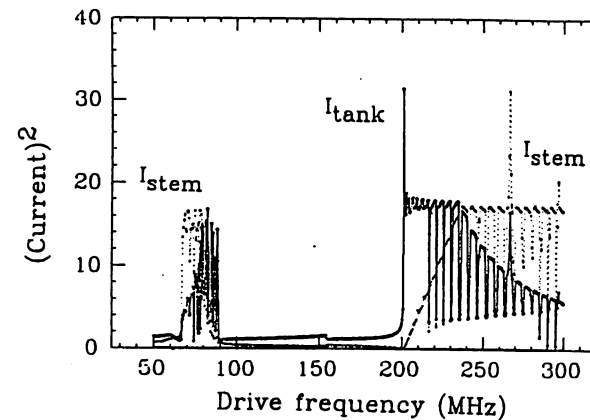
Fig. 63 Calculated sums of I_{tank} and I_{stem} for the 35-cell post-less tank vs. drive frequency ω. Used parameters are given in section 10.1.
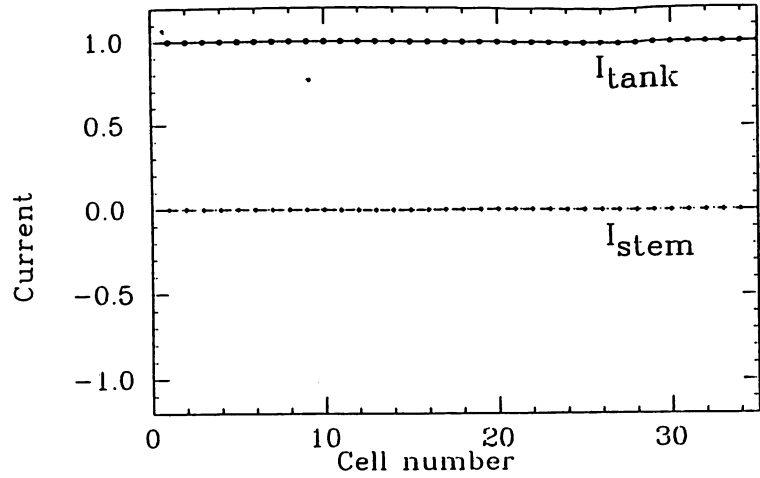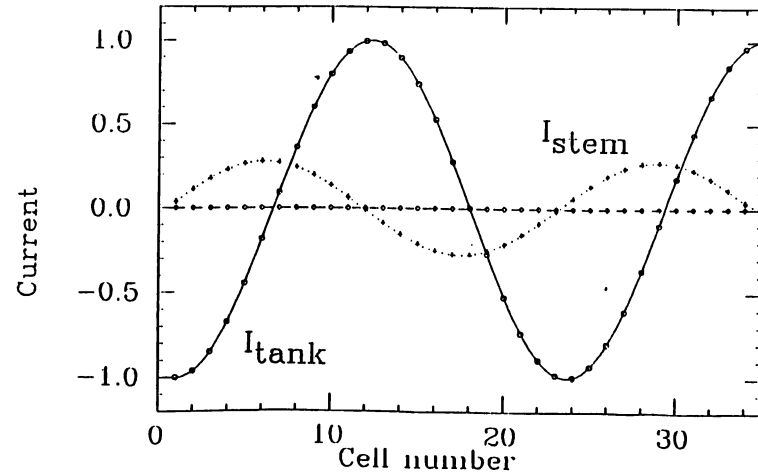
a) TM010-like.
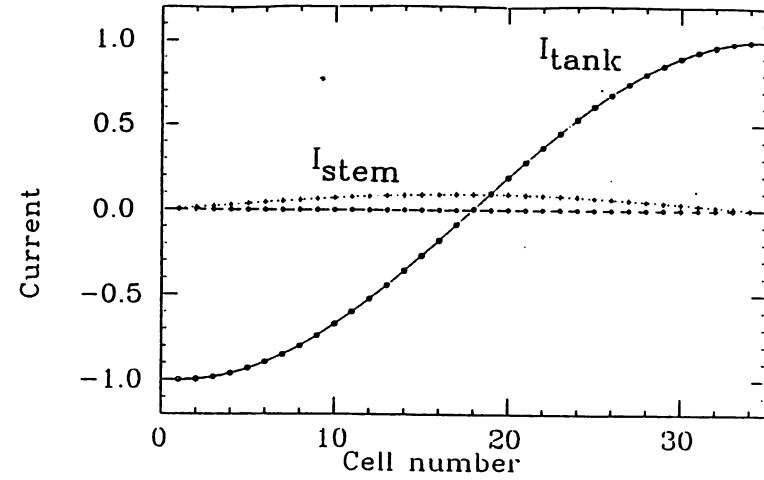
b) TM011-like.
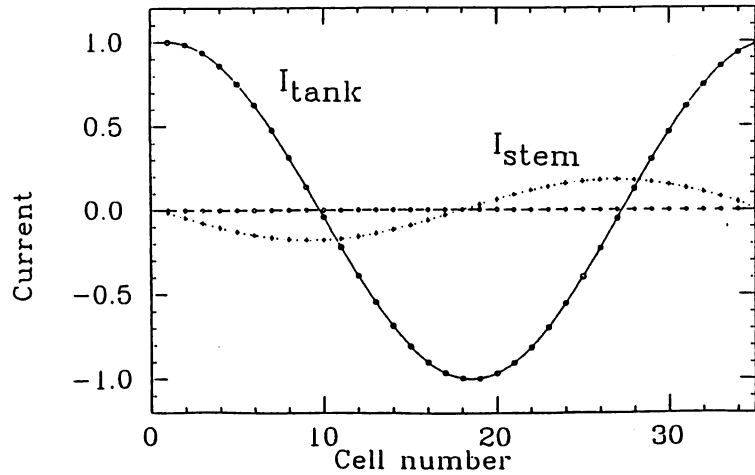
c) TM012-like.

d) TM013-like.

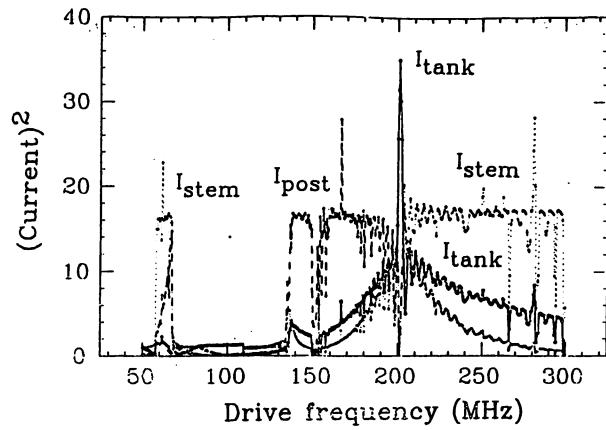Fig. 64 Example of the field distribution of post-less circuits.

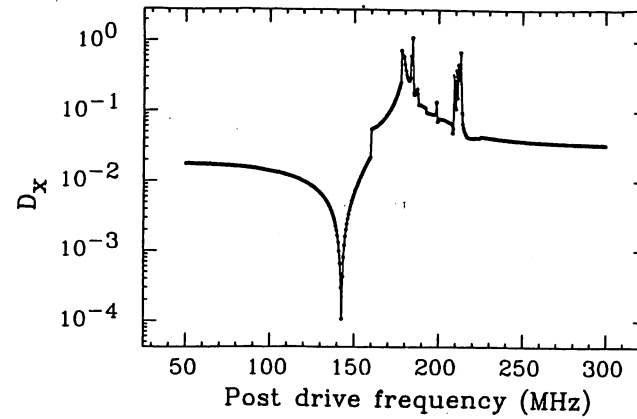Fig. 65 Calculated sums of I_{tank}, I_{stem} and I_{post} during stabilization vs. drive frequency ω. $\omega_2 = 142.4$.

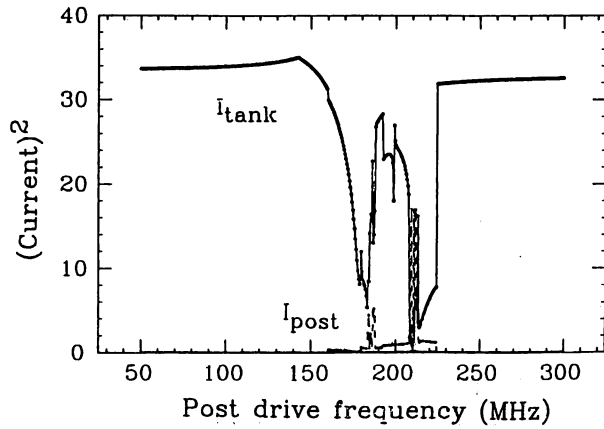Fig. 66 Calculated distortion parameters vs. post drive frequency ω_2.

Fig. 67 Calculated sums of square of $I_{tank}(n)$, $I_{stem}(n)$ and $I_{post}(n)$ vs. post drive frequency ω_2.
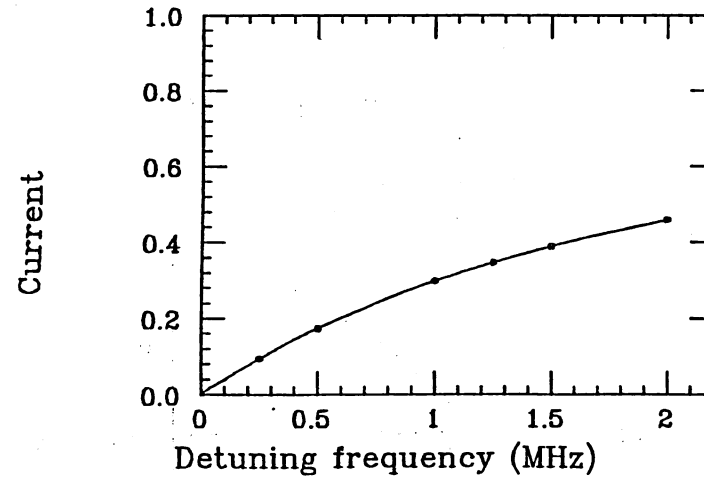

Fig. 68 Calculated sum of I_{post} during stabilization vs. the perturbation given to both end circuits.